

# General Aviation Radar System for Navigation and Attitude Determination

*Deriving aircraft states using multiple on board FMCW radars*

C. Naulais

August 10, 2015



# **General Aviation Radar System for Navigation and Attitude Determination**

**Deriving aircraft states using multiple on board FMCW radars**

MASTER OF SCIENCE THESIS

For obtaining the degree of Master of Science in Aerospace Engineering  
at Delft University of Technology

C. Naulais

August 10, 2015



**Delft University of Technology**

Copyright © C. Naulais  
All rights reserved.

DELFT UNIVERSITY OF TECHNOLOGY  
DEPARTMENT OF  
CONTROL AND SIMULATION

The undersigned hereby certify that they have read and recommend to the Faculty of Aerospace Engineering for acceptance a thesis entitled “**General Aviation Radar System for Navigation and Attitude Determination**” by **C. Naulais** in partial fulfillment of the requirements for the degree of **Master of Science**.

Dated: August 10, 2015

Readers:

---

prof.dr.ir. J. M. Hoekstra

---

ir. R. N. H. W. van Gent

---

dr.ir. G. N. Saunders



---

# Acronyms

<b>AGL</b>	Above Ground Level
<b>ASI</b>	Air Speed Indicator
<b>CA</b>	Collision Avoidance
<b>CAR</b>	Collision Avoidance Radar
<b>CAS</b>	Calibrated Airspeed
<b>D&amp;A</b>	Detect & Avoid
<b>DEM</b>	Digital Elevation Map
<b>DNS</b>	Doppler Navigation System
<b>ED&amp;A</b>	Electronic Detect & Avoid
<b>FMCW</b>	Frequency Modulated Continuous Wave
<b>GUI</b>	Graphical User Interface
<b>IAS</b>	Indicated Airspeed
<b>IFR</b>	Instrument Flight Rules
<b>IMU</b>	Inertial Measurement Unit
<b>MSL</b>	Mean Sea Level
<b>PRF</b>	Pulse Repeat Frequency
<b>RMS</b>	Root Mean Square
<b>S&amp; A</b>	See & Avoid
<b>STRM</b>	Shuttle Radar Topography Mission
<b>TAS</b>	True Airspeed
<b>VFR</b>	Visual Flight Rules
<b>VMC</b>	Visual Meteorological Conditions
<b>VR</b>	Velocity-Range



---

# List of Symbols

## Greek Symbols

$\alpha$	Angle of attack
$\alpha_r$	Radar depression angle
$\beta$	Drift angle
$\beta_r$	Radar azimuth angle
$\epsilon$	Error
$\theta$	Pitch angle
$\lambda$	Longitude
$\tau$	Time delay
$\Phi$	Phase
$\Phi$	Latitude
$\phi$	Roll angle
$\chi$	Velocity frequency
$\psi$	Heading angle
$\omega$	Angular frequency

## Roman Symbols

<b>B</b>	Bandwidth
<b>c</b>	Speed of light
$F_b$	Body-fixed reference frame
$f_c$	Central frequency
$f_d$	Doppler shift

$F_E$	Earth-fixed reference frame
$f_r$	Received frequency
$f_s$	Sample frequency
$f_t$	Transmitted frequency
$\mathbf{h}$	Height
$\mathbf{K}$	Number of modulations
$R_{max}$	Maximum radar range
$\mathbf{s}$	Distance
$\mathbf{T}$	Period
$t_g$	Guard time
$\mathbf{v}$	Velocity
$v_{gs}$	Ground speed
$x_b$	Beat signal
$x_r$	Received signal
$x_t$	Transmitted signal
$x_v$	Video signal

---

# Contents

<b>Acronyms</b>	<b>v</b>
<b>List of Symbols</b>	<b>vii</b>
<b>1 Abstract</b>	<b>1</b>
<b>2 Introduction</b>	<b>3</b>
<b>3 Background Information</b>	<b>5</b>
3-1 Frequency Modulated Continuous Wave Radar . . . . .	5
3-1-1 Signal processing . . . . .	7
3-1-2 Velocity-range spectrum . . . . .	9
3-2 Visual Flight Rules . . . . .	10
3-2-1 See and avoid . . . . .	10
3-2-2 Navigation . . . . .	10
3-2-3 Attitude determination . . . . .	13
3-3 Doppler Navigation Systems . . . . .	15
3-3-1 Antenna orientation matrix . . . . .	16
3-4 Attitude and height determination . . . . .	17
3-4-1 Two-dimensional example . . . . .	17
3-4-2 Three-dimensional problem . . . . .	19
3-4-3 Plane fitting . . . . .	20
3-5 Velocity Determination . . . . .	20
3-5-1 Overdetermined system . . . . .	21

<b>4</b>	<b>Problem Statement</b>	<b>23</b>
4-1	Navigation and Attitude Determination . . . . .	23
4-2	Beam Width . . . . .	24
4-3	Terrain Ambiguity . . . . .	25
4-4	Radar Configuration . . . . .	26
4-5	Python model . . . . .	26
4-6	Research Question . . . . .	26
<b>5</b>	<b>Simulator in Python</b>	<b>29</b>
5-1	Flight Data Acquisition . . . . .	30
5-2	Doppler Navigation System Model . . . . .	31
5-2-1	Graphical user interface . . . . .	31
5-2-2	Radar initialization module . . . . .	32
5-2-3	Velocity-range data acquisition module . . . . .	33
5-2-4	Signal generation module . . . . .	34
5-2-5	Signal processing module . . . . .	35
5-2-6	State derivation module . . . . .	36
5-3	Digital Elevation Map . . . . .	37
<b>6</b>	<b>Results</b>	<b>39</b>
6-1	Flight Data . . . . .	39
6-2	Radar Configuration . . . . .	39
6-2-1	Individual antenna orientation . . . . .	39
6-2-2	Standard radar configuration . . . . .	40
6-3	Graph Explanation . . . . .	40
6-4	Effect of Beam Width . . . . .	41
6-5	Effect of Radar Depression Angle . . . . .	43
6-5-1	Flat Earth . . . . .	44
6-5-2	Non-flat Earth . . . . .	45
6-6	Effect of Antenna Azimuth Angle . . . . .	47
6-7	Effect of Terrain . . . . .	48
6-8	Navigation and Attitude Determination Performance . . . . .	49
6-8-1	Horizontal navigation performance . . . . .	50
6-8-2	Vertical navigation performance . . . . .	53
6-8-3	Attitude determination performance . . . . .	53
6-9	Optimal Radar Configuration . . . . .	53
<b>7</b>	<b>Conclusion</b>	<b>55</b>

---

<b>8 Recommendations</b>	<b>59</b>
8-1 Improve the terrain error . . . . .	59
8-2 Flight data acquisition . . . . .	59
8-3 Signal processing . . . . .	60
8-4 Graphical User Interface . . . . .	60
8-5 Simulation improvements . . . . .	61
<b>A Flight data</b>	<b>63</b>
<b>B Simulation results</b>	<b>67</b>
<b>C Doppler ambiguity</b>	<b>75</b>
<b>Bibliography</b>	<b>77</b>



---

# Chapter 1

---

## Abstract

General Aviation aircraft mostly fly with Visual Flight Rules (VFR). These are rules in aviation that permit the pilot to fly on sight if the weather conditions offer enough visibility for the pilot to perform the following tasks visually: collision avoidance with terrain or other airborne object, navigation and attitude determination. VFR flight is therefore a very independent way of flying requiring very few on-board instruments, but it is very dependent on weather conditions.

Selfly Electronic Detect and Avoid has therefore developed a Collision Avoidance Radar that can support the pilot to detect and avoid the ground and airborne objects. This Frequency Modulated Continuous Wave radar is small, lightweight and can be mounted almost anywhere on the aircraft.

This thesis researched if the radar could also be used as Doppler Navigation System to support the pilot for navigation and attitude determination. A method is proposed which uses the radar data of multiple on-board radars to calculate the aircraft states required for navigation and attitude determination. With this method the height, the roll angle and the pitch angle can be determined with the range measurements and the aircraft velocity vector in the body-fixed reference frame can be calculated using the velocity measurements. Assuming a known heading angle, the ground speed of the aircraft can also be determined.

The Doppler Navigation System was modeled in Python and flight data was generated with the flight simulator X-Plane 9. The model was used to determine how the aperture angle would affect the accuracy of the obtained states required for navigation and attitude determination and what the optimum on-board radar configuration is.

Navigation with the DNS showed an error in the horizontal position of  $455m$  for a flight of  $728s$  in which the aircraft traveled  $84.339km$ . The height of the aircraft can be determined within  $20m$  of the actual height of the aircraft along the whole flight. The obtained roll angle was always within  $1^\circ$  of the actual roll angle when smaller than  $10^\circ$  and the pitch angle error never exceeded  $1^\circ$ . These result show that this system could be used to navigate with no visibility conditions for a short duration, for example when trapped in a cloud.

These results were obtained for a flight over the Dutch coast using a Digital Elevation Map with an accuracy of 3 arc seconds. The DNS performed best with radars with a low depression angle and the azimuth angle did not appear to significantly influence the accuracy of the states. The terrain was however the largest source of error, as the method to calculate the states assumes a flat Earth.

The modeling of the radar signal was too computationally intensive to be integrated in the model, therefore the ground velocity and range measurements are assumed to be perfect.

In order to improve the accuracy of the system, terrain recognition could be added which would allow the system to determine three or more geographic positions on the surface and use these positions to geometrically determine its position and attitude using triangulation.

---

## Chapter 2

---

# Introduction

In the early days of aviation, pilots primarily relied on sight to fly aircraft, with the use of basic instruments to indicate states such as altitude and airspeed. This is also known as flying with Visual Flight Rules (VFR) and is still the way general aviation aircraft fly today. The instruments were, and still are pressure sensing devices giving the pilot the dynamic pressure indicating the airspeed, and the static pressure for pressure altitude. Later, radio navigation and gyroscopic instruments were added to enable flying without sight, or so called Instrument Flight Rules (IFR) flight. The principle of measuring several different variables (pressures, gyroscopic angles, radio beacon bearings and distances etc.) to indicate the various flight states such as altitude, airspeed and position on a map made aviation a very inductive process.

In VFR flight the process has remained the same over time. Without the use of many sensors, it is still possible to fly on sight like in the early days of aviation if the weather conditions allow for sufficient visibility. With an altimeter and air speed indicator, the pilot should be able to perform the tasks of navigation, object and terrain avoidance, and aircraft attitude determination, on sight. Landmarks are used to determine the aircraft position and the horizon is a reference for the aircraft attitude. Collision avoidance with the ground and other aircraft is done by looking out the cockpit windows. VFR flight is therefore a very independent way of flying not even requiring ATC communication in some airspace. However, VFR flight is dependent on the pilot's visibility, which is limited by the weather and the angle of view the cockpit windows offer. Mid-air collisions occur more often than any other branch of aviation because pilots have a limited view of what happens behind the aircraft. Reduced visibility due to sudden cloud formation can result in the pilot being unable to navigate or determine the aircraft attitude.

In an attempt to fly VFR independently without having the limitations of weather conditions and cockpit visibility limitations, Selfly Electronic Detect & Avoid (ED&A) has designed an on-board Collision Avoidance Radar (CAR) to replace the human vision in VFR flight. The primary task of this 10GHz Frequency Modulated Continuous Wave (FMCW) radar is to independently detect the ground and airborne objects in any weather. The use of radars could support or replace the pilot for the tasks of navigation and attitude determination

in VFR flight with non-VFR weather conditions. The Collision Avoidance performance of the radar is being researched by Selfly ED&A. This thesis will research if the CAR can also support the pilot in navigation and attitude determination through direct measurement of the aforementioned variables as opposed to the current state of induction and inference of the variables. Thereby achieving an 'Electronic'-VFR flight which relies on the sight of the radar instead of the human pilot.

The goal of this thesis is to design a system that can support the pilot to navigate and determine the aircraft attitude in degraded weather conditions. This has to be done using multiple on-board radars developed by Selfly ED&A. The FMCW radar measures both distance and velocity and can therefore be used both as Doppler radar and radio altimeter. The on-board radars form a Doppler Navigation System (DNS) that uses multiple relative radial velocity and distance measurements to determine the aircraft states required for navigation and attitude determination. The CAR used in the DNS is not designed for these tasks, so this thesis will investigate the performance of the system when determining the aircraft horizontal and vertical position as well as its attitude angles. This thesis will also try to optimize the DNS parameters such as the configuration of on-board transmitters and receivers for this system and quantify the effect of the CAR on the navigation error.

The first part of this report gives the reader background information on FMCW radars and how the distance and relative radial velocity of multiple object with respect to the radar can be determined. Then the aircraft states required for navigation and attitude determination in VFR flight are described and the method to obtain these states using velocity and distance measurements is explained. The following part is the problem statement and research question describing the challenges faced when using the CAR for this purpose. This is followed by an explanation of the Python model created for this thesis. The results show the performance of the system for three simulated flights with varying on-board radar configurations. After the results, the conclusion and recommendation chapters summarize and give advice on the direction of further research in this field.

# Background Information

Section 3-1 describes how FMCW radars can be used to measure the velocity and range of multiple objects. Section 3-2 explains the requirements for VFR flight in general aviation where the pilot has to visually Detect & Avoid (D&A), determines the attitude and navigate the aircraft. This is followed by a method to support the pilot in these tasks using multiple on-board FMCW radars in a DNS.

### 3-1 Frequency Modulated Continuous Wave Radar

The Collision Avoidance Radar developed by Selfly ED&A is a Frequency Modulated Continuous Wave radar. FMCW radars send out and receive a continuous signal which is periodically modulated in frequency. They are used to measure the relative radial velocity of objects and the distance between the radar and the objects (Skolnik, 2001), (Hyun, Oh, & Lee, 2012). This is done continuously for multiple objects in range of the radar. The range of the radar is defined as the minimum distance an object can have without being detected and the aperture angle of the radar. The following section describes how a FMCW emits a signal and uses the echo of that signal to determine this velocity and distance.

A FMCW radar is composed of a signal generator, a transmitter and a receiver. Figure 3-1 shows the schematic representation of a FMCW radar. The signal generator generates a continuous signal which is passed on to the transmitter antenna. This transmitted signal  $x_t$  is periodically modulated in frequency. This means the modulation repeats itself for every Time Period  $T$ . The modulation can vary in shape, several examples are sine, cosine, sawtooth or triangle shapes. In this research the sawtooth modulation is applied. So,  $x_t$  is defined as a sine with a frequency that which is a function of time (Undheim, 2012).

$$x_t = A \sin \Phi_t(t) \quad (3-1)$$

Where  $\phi_t$  is the phase of the transmitted signal and  $A$  is the amplitude of the signal.

The frequency is the derivative of the phase of the signal.

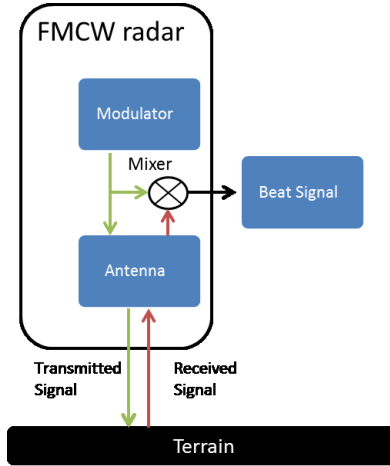


**Figure 3-1:** Schematic diagram of a FMCW radar sending a signal towards the ground which is perfectly reflected. The received signal is mixed with a copy of the transmitted signal to form the beat signal.

$$f(t) = \frac{1}{2\pi} \frac{d\Phi(t)}{dt} \quad (3-2)$$

In case of a sawtooth signal, the frequency of  $x_t$  is a linear periodic function increasing linearly over time, from central frequency  $f_c$  with Bandwidth  $B$  over Time Period  $T$ :

$$f_t(t) = f_c + \frac{B}{T}t_k \quad (3-3)$$

Where  $f_t$  is the frequency of  $x_t$ .

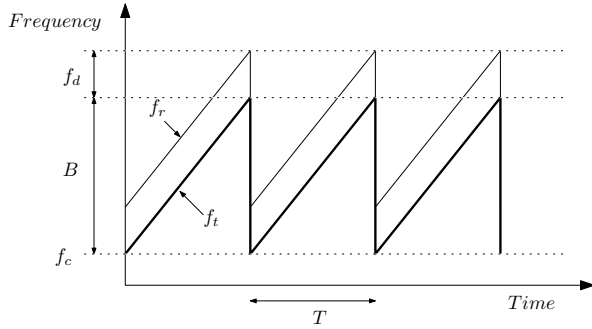
With  $t_k$  as the time of each period.

$$t_k = 0 < t < T \quad (3-4)$$

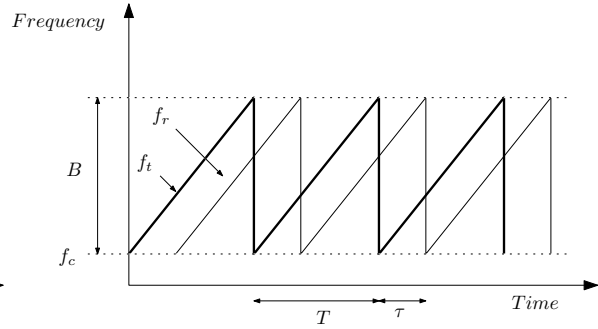
Next, the signal is echoed back and reaches the receiver. The frequency  $f_r$  of the received signal is different than  $f_t$  due to the Doppler shift, which is caused by the relative radial velocity of the target with respect to the radar, and a time shift, due to the distance to the target. The frequency of the transmitted signal and the received signal are plotted over time in Figure 3-2 and Figure 3-3.

Figure 3-2 and Figure 3-3 also illustrate the effect of the range and velocity of a target on the radar signal. The example above represents a single target. The relative radial velocity causes a shift in frequency which is the Doppler shift  $f_d$  (Raney, 1971). The Doppler shift is a function of the velocity  $v$ , speed of light  $c$  and the transmitted frequency  $f_t$ . The transmitted frequency is assumed constant because its variation is negligible. When the velocity of the target is much smaller than the speed of light, the Doppler shift can be approximated as follow:

$$f_d = \frac{2v}{c} f_t \quad (3-5)$$



**Figure 3-2:** The velocity of the object causes a frequency shift in the received signal  $f_r$  compared to the transmitted frequency  $f_t$ . This frequency shift is equal to the Doppler shift  $f_d$



**Figure 3-3:** The range of the object causes a time shift of the received frequency  $f_r$  compared to the transmitted frequency  $f_t$ . The time shift is the time it takes for the signal to travel back and forth from the radar to the object.

The distance causes a shift in time  $\tau$ . This  $\tau$  is the time it takes for the signal to reach the target and come back. It is a function of the distance to the target  $s$  and the speed of light  $c$ .

$$\tau = \frac{2s}{c} \tag{3-6}$$

Taking  $f_d$  and  $\tau$  into account, the received frequency  $f_r$  can be described as:

$$f_r(t_k) = f_t - \frac{B}{T}\tau + f_d \tag{3-7}$$

Then a copy of  $x_t$  is mixed with the  $x_r$  resulting in the beat signal  $x_b$ .  $x_b$  is described as:

$$x_b = A \sin \Phi_b(t) \tag{3-8}$$

With:

$$\Phi_b = \Phi_t - \Phi_r \tag{3-9}$$

Signal  $x_b$  is the signal containing range and velocity information.

### 3-1-1 Signal processing

The received signal is mixed with a copy of the transmitted signal, resulting in the beat signal  $x_b$ . This section will describe the signal processing performed on  $x_b$  to retrieve velocity and range information from multiple targets. According to the two dimensional signal processing technique described by Wotjkiewicz et al. (Wojtkiewicz, Misiurewicz, Nałecz, Jedrzejewski, & Kulpa, 1997), the signal processing is done over  $K$  modulations, such that the total integration time is  $KT$  seconds. In this time interval, the velocity of the aircraft is assumed constant and the distance of the target towards the radar can be calculated as follow:

$$s = s_0 + vTk \text{ for } k = 0, 1, \dots, K - 1 \tag{3-10}$$

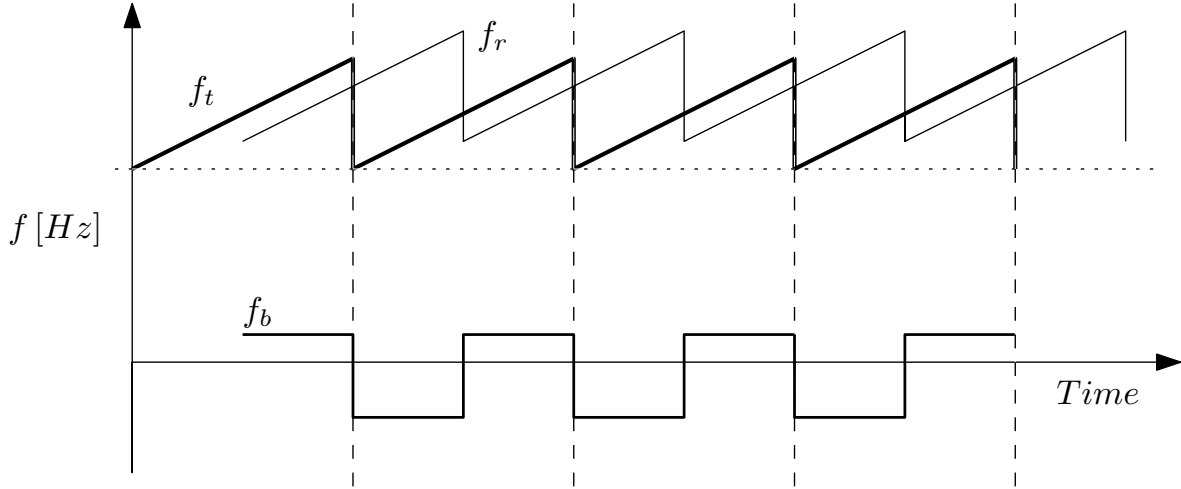


**Figure 3-4:** Example of the transmitted frequency  $f_t$  of four modulation periods of a sawtooth signal with the received frequency  $f_r$  of a moving object. The beat frequency  $f_b$  is the frequency of the beat signal  $x_b$ .

Where  $s$  is the distance or range of the target and  $s_0$  is the distance at  $t = 0$ .

$\tau$  can therefore be written as:

$$\tau = \tau_0 + \frac{2}{c} (vkT) \quad (3-11)$$

This means that the phase  $\Phi_b$  of the beat signal  $x_b$  can be rewritten as:

$$\Phi_b = 2\pi \left[ \tau_0 f_c + k f_d T + \left( f_d + \frac{B}{T} \tau \right) t_k \right] \quad (3-12)$$

A guard time  $t_g$  is introduced so the received signal of the preceding pulse does not interfere with the measurement. The guard time is calculated using the maximum range  $R_{max}$ .

$$t_g = \frac{2R_{max}}{c} \quad (3-13)$$

The received signal and a copy of the transmitted signal are mixed resulting in the video signal  $x_v$ . Next a 2D Fourier transform is performed on  $x_v$  to compute the Doppler shift - Range profiles. The first Fourier transform is performed on the signal sampled with  $f_s$ , with an N-point DFT for every period T.

$$X_b(\omega, k) = \int_{t_g}^T x_b(t) e^{-j\omega t} dt \quad (3-14)$$

The spectrum  $X_r(\omega, k)$  contains the range information of each target as a discrete function of  $k$ . It is stored in N range bins with a size of  $\Delta R = \frac{R_{max}}{N}$ . The range increases or decreases over  $k$  relative to the velocity of the target, due to the Doppler shift. The following discrete Fourier transformation uses  $K$  samples at  $T$  intervals. This means the sampling frequency is equal to the Pulse Repeat Frequency (PRF).

$$X(\omega, \chi) = \sum_{k=0}^{K-1} X_b(\omega, k) e^{-jk\chi} \quad (3-15)$$

The second Fourier transform yields a spectrum where the maximum absolute value of the spectrum is defined as  $\chi_d$  and is equivalent to  $\chi_d = 2\pi F_d T$ . The Doppler shift corresponding to each range can then be calculated and this is transformed into a Velocity-Range (VR) map using the Doppler shift equation.

### 3-1-2 Velocity-range spectrum

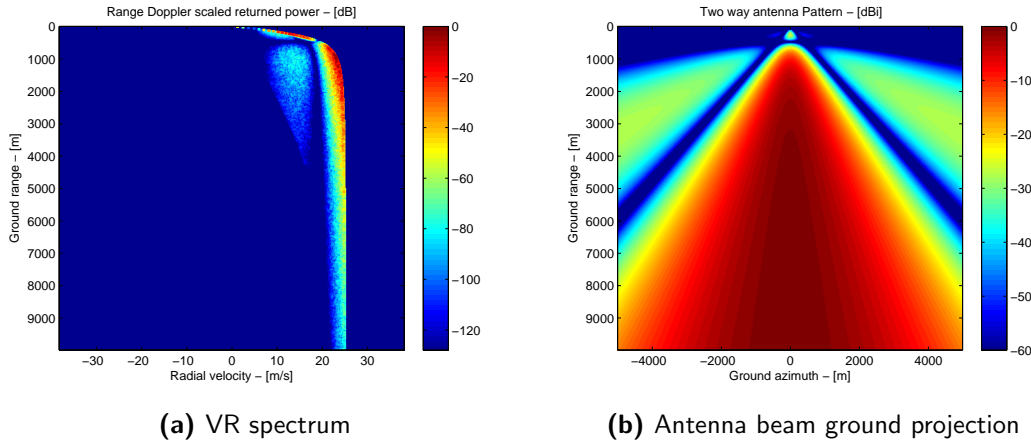


**Figure 3-5:** On the left, the velocity-range spectrum of a radar oriented along the longitudinal axis of the aircraft. The antenna beam ground projection is represented on the right. The aircraft flies horizontally with a velocity of  $25m/s$ , therefore, the maximum speed measured on the VR map is  $25m/s$ .

The data resulting from the transformation is a 2D spectrum with the range the y-axis and the relative radial velocity on the x-axis. An example of such a VR map is given in Figure 3-5a. This VR map is created with a FMCW radar mounted on the wing of an aircraft. The radar is oriented along the longitudinal axis of the aircraft and the aircraft flies horizontally at a height of  $400m$  with a velocity of  $25m/s$ . Figure 3-5b shows the antenna beam pattern on the ground below the aircraft. The horizontal position of the aircraft is  $(0,0)$  in Figure 3-5b.

Both the velocity and range are functions of frequency; the velocity is a function of the velocity frequency and the range of the range frequency which are determined with the Fourier transformation. The maximum and minimum velocity on the axis are the velocities corresponding to the frequencies  $\frac{PRF}{2}$  and  $-\frac{PRF}{2}$ . This is due to the Nyquist criterion which is further explained in Appendix C.

As can be seen in Figure 3-5a the maximum measured radial velocity of the ground clutter is  $25m/s$  which is the velocity of the aircraft. The maximum and minimum velocity of the axis is the velocity which the The distance measured has an error due to the Doppler shift therefore the minimum range measured is slightly smaller than the height of the aircraft. As

can be seen in Figure 3-5b the radar beam covers a large area of ground. However, the radar measurements of the image can be located with an accuracy of  $10^\circ$  using the phase difference of multiple received signals. It is therefore possible to model the FMCW radar as multiple radars with a  $10^\circ$  aperture angle. This assumption is used throughout the thesis.

## 3-2 Visual Flight Rules

Visual Flight Rules are rules defined by aviation regulatory agencies permitting aircraft to fly on sight and uncontrolled. VFR flight is allowed only under certain weather conditions, such as minimum visibility conditions called Visual Meteorological Conditions (VMC), and in specific airspace. During VFR flight, the pilot has to be able to perform three tasks visually: See and avoid other airborne objects and the ground, navigate the aircraft with the ground as reference, and determine the attitude of the aircraft (ICAO, 1990).

Aircraft flying VFR are mostly General Aviation aircraft. Scheduled air services provided by airlines usually fly IFR, since they need to be able to operate under all visibility conditions. Therefore their flight is based on instrument references instead of vision and they fly in controlled airspace. VFR flight requires very few instruments on board, and a pilot can fly independently of other airspace users. In uncontrolled airspace, the pilot is normally not dependent on ATM systems to fly.

It frequently occurs that pilots become trapped due to sudden cloud formation, forcing the pilot to fly blindly through clouds towards areas with better visibility. This is an extremely dangerous situation as the pilot has no vision while flying through a cloud and can therefore not navigate, see and avoid, and determine the aircraft attitude (Dale & Teresa, 2003). It can take up to several minutes to fly through a cloud before regaining VMC.

### 3-2-1 See and avoid

See and Avoid is the VFR term for Collision Avoidance (CA). As the name suggests, the pilot looking out the cockpit windows does See and Avoid (SA) visually. The two main tasks of See & Avoid (S& A) are: separation with other airborne objects, and terrain collision avoidance. Separation with other aircraft is done following the guidelines set by ICAO in Annex 2, Rules of the air (ICAO, 1990). This annex describes aircraft operations such as right of way and other aircraft interaction in the air.

Terrain avoidance is generally done by looking out the window. To know the exact altitude of the aircraft, the pilot has an altimeter which measures the pressure altitude of the aircraft. As collision avoidance is the main focus of the radar project of Selfly ED&A it is left out of the scope of this report and the focus lies on navigation and attitude determination.

### 3-2-2 Navigation

According to literature, the definition of navigation is: "Navigation is the process of piloting an aircraft from one geographic position to another while monitoring one's position as the flight progresses." (FAA, 2014). The position of the aircraft on the earth is the geodetic

location and the altitude. It is defined as the geographic coordinates (latitude  $\Phi$ , longitude  $\lambda$ ) and elevation above Mean Sea Level (MSL) of the aircraft. In VFR flight, the pilot determines its horizontal position and heading using known landmarks. The exact elevation is read from a barometric altimeter and the velocity is given by the Air Speed Indicator (ASI).

**Dead-reckoning navigation** Dead-reckoning navigation is a way to navigate requiring the velocity and the heading of the aircraft. It requires a known initial position and knowledge of the wind speed and direction. The pilot can then calculate the distance traveled over time and because the direction is also known, this can be added to the initial position. Dead-reckoning navigation requires a very precise velocity and heading because errors grow over time.

In VFR flight, the pilot keeps a desired heading by recognizing landmarks and compensating for the drift. The drift caused by the wind causes the heading of the aircraft not to be the actual heading of the ground track. This is explained in paragraph 3-2-2. In VFR flight the drift is determined using the known aircraft speed and comparing the position reached over time with the expected position. It can also be calculated using the effect of the wind speed and direction over time. The drift is taken into account by the pilot to adjust the heading required to fly the desired trajectory.

The velocity of the aircraft can be measured with different references. The velocity measured by the aircraft pressure based instruments is the velocity of the aircraft with respect to the air mass it is flying in. The velocity of the aircraft with respect to the ground is called the ground speed. The vertical speed is the change in aircraft elevation and is also known as the rate of climb. This velocity also has the Earth as reference point.

**True airspeed** The True Airspeed (TAS) is the velocity of the aircraft with respect to the air mass it is flying in. The TAS is not directly measured, nor is it indicated in the aircraft but instead the ASI displays the Indicated Airspeed (IAS). The IAS is calculated using only the dynamic pressure and it indicates speeds relevant for the aircraft aerodynamic performance such as stall speed, landing speed and take-off speed. The IAS is important to keep the aircraft in its flight envelope but does not give direct information on the actual speed of the aircraft. The speed the aircraft would have flying at MSL is called the Calibrated Airspeed (CAS). This is the IAS corrected for the instruments. The CAS is the TAS the aircraft would have at MSL.

The actual speed of the aircraft relative to the air mass it is flying in is called the TAS. It is the CAS corrected for altitude and air compressibility effects. This speed is calculated using the total pressure, the static pressure and the total air temperature with Equation 3-16

$$TAS = \sqrt{\frac{2\gamma RT_0}{\gamma - 1} \left[ \left( \frac{p_1}{p_2} \right)^{(\gamma-1)/\gamma} - 1 \right]} \quad (3-16)$$

**Ground speed** The aircraft has a TAS which is the speed of the aircraft with respect to the mass of air it is flying in. To calculate the speed of the aircraft relative to the Earth, the wind speed and direction have to be known. The horizontal component of the TAS is added to the horizontal component of the wind speed resulting in the ground speed or ground track. The

TAS is defined in the body-fixed reference frame, and has to be transformed to the Earth-fixed reference frame using the Euler angles(see section 3-2-3). The drift angle is the angle between

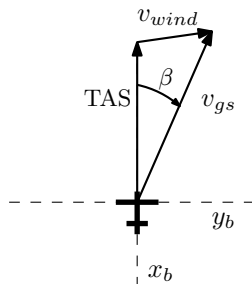


**Figure 3-6:** The ground speed  $v_{gs}$  is the sum of the wind speed  $v_w$  and the True Air Speed (TAS). The drift angle  $\beta$  is the angle between the ground speed and the longitudinal axis of the aircraft  $x_b$ .

the heading of the aircraft and the aircraft ground track or the aircraft heading. The drift angle is caused by the wind and is determined in VFR by visually comparing the heading of the aircraft with the actual flown path using landmarks.

**Rate of climb** The rate of climb of the aircraft is the change in altitude of the aircraft, or the vertical component of the velocity vector in the Earth-fixed reference frame. Combining the ground speed and the rate of climb gives a 3D vector of the aircraft velocity in the Earth-fixed reference frame. This vector is not aligned with the aircraft body. The horizontal deviation, caused by the wind is the drift angle. The vertical deviation is caused by the aerodynamic properties of the wings and is called the angle of attack.

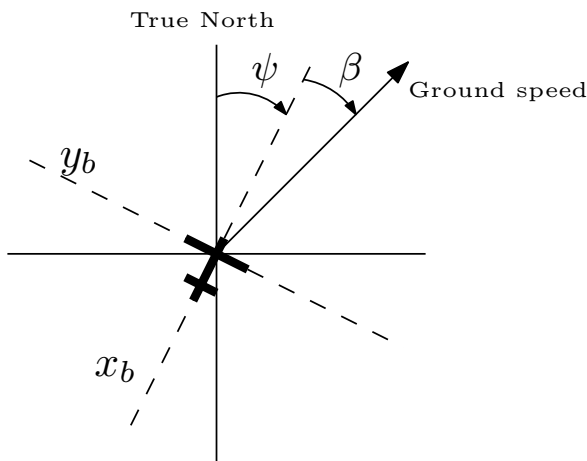


**Figure 3-7:** The aircraft heading  $\psi$  is the angle between the longitudinal axis  $x_b$  of the aircraft and the true North which is the  $x$ -axis of the earth-fixed reference frame  $x_E$ . The drift angle  $\beta$  is the angle between the ground speed  $v_{gs}$  and the aircraft heading.

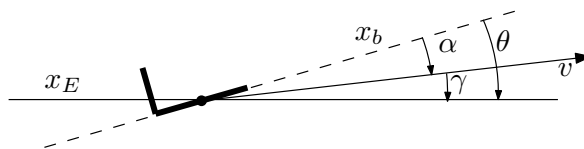


**Figure 3-8:** The angle of attack  $\alpha$  is the angle between the flight path and  $x_b$ . The flight path angle  $\gamma$  is the angle between the flight path and  $x_E$ . The pitch angle is therefore:  $\theta = \alpha + \gamma$ .

The angle of attack is the angle between the  $x_b$  - axis and the projection of the velocity vector

on a plane perpendicular to  $y_b$ . It is a measure for the aircraft orientation in the air flow. It can be used to calculate the flight path angle if  $\theta$  is known, as is shown in Figure 3-8. The angle of attack is measured using a sensor that measures the direction of the wind flow along the fuselage of the aircraft, or with an Inertial Measurement Unit (IMU).

### 3-2-3 Attitude determination

Aircraft attitude is the relative orientation of the aircraft with respect to the Earth. In VFR flight, the pilot can determine the attitude of the aircraft by looking at the horizon and the position of the horizon with respect to the cockpit. The aircraft attitude is described with three angles, these are the Euler angles. The three Euler angles: roll angle  $\phi$ , pitch angle  $\theta$ , and heading angle  $\psi$ , also describe the angular difference between the Earth-fixed reference frame  $F_E$  and the body-fixed reference frame  $F_b$  (Diebel, 2006).

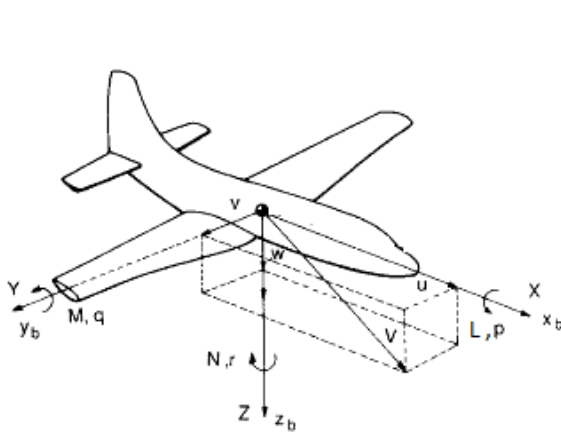


Figure 3-9: Body-fixed reference frame

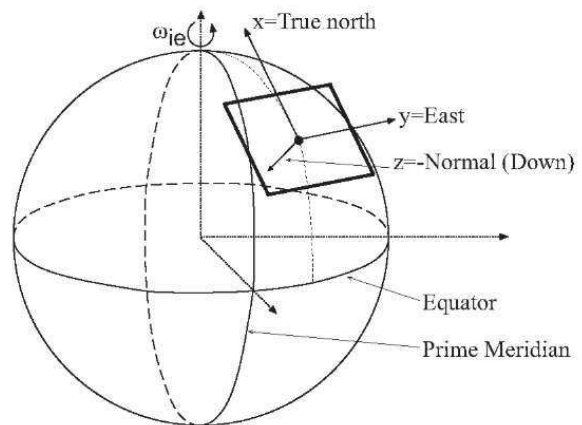
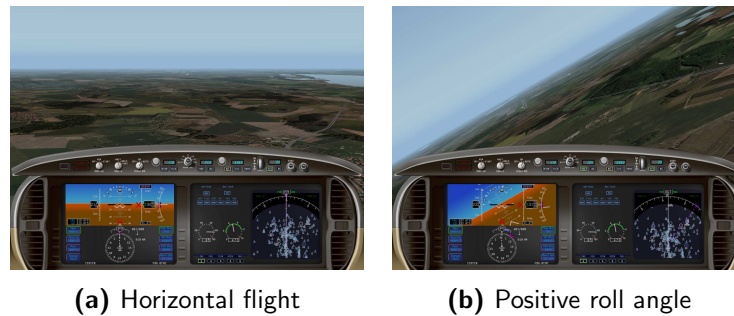


Figure 3-10: Earth-fixed reference frame

**Body-fixed reference frame** The body-fixed reference frame shown in Figure 3-9 is a right handed coordinate system with the origin at the center of the aircraft. The x-axis is running along the aircraft longitudinal axis, positive through the nose. The y-axis is oriented towards the right wing of the aircraft and the z-axis is positive downwards. The orientations and positions of the different radar are defined in this reference frame.

**Earth-fixed reference frame** The Earth-fixed reference frame shown in Figure 3-10) is also a right handed coordinate system. It is defined with the origin at the aircraft center. The x-axis is pointing North, the z-axis points West, and the z-axis points down. This reference frame is used for navigation to determine the speed and the position of the aircraft with respect to the Earth. It is also used to model the beams and the terrain under the aircraft.

**Roll angle** The roll angle  $\phi$  describes a rotation of the longitudinal axis of the aircraft. The roll is clockwise positive, meaning a positive roll results in a right turn of the aircraft. In VFR the pilot determines the roll angle comparing the horizon with horizontal references in



**Figure 3-11:** Pilot view of a roll motion

the aircraft. A pilot can easily detect the difference of even  $1^\circ$  or  $2^\circ$  roll if the aircraft flies horizontally. However, in a roll of  $20^\circ$  or  $30^\circ$ , a  $1^\circ$  difference is not easy to distinguish.

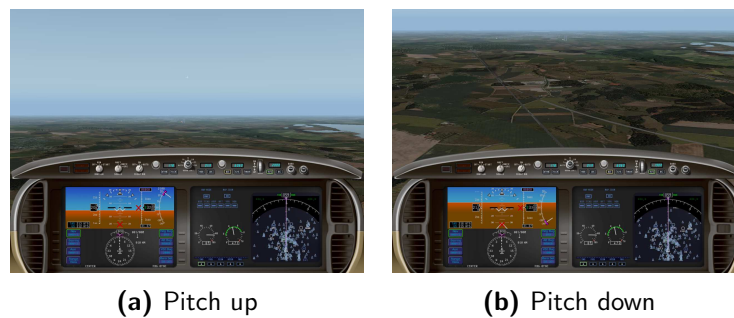


**Figure 3-12:** Pilot view of a pitch motion

**Pitch angle** The pitch angle  $\theta$  describes a rotation of the lateral axis of the aircraft. A positive pitch means the aircraft points its nose upwards with respect to the earth. A pilot can determine the pitch of the aircraft by looking at the horizon. When pitching up, the horizon will appear to be lower and the pilot will see more sky than land.

**Heading angle** The heading angle  $\psi$  describes a rotation of the vertical axis of the aircraft. This angle describes the orientation of the aircraft with respect to the geographic North where  $90^\circ$  is a West heading,  $180^\circ$  is a South heading, and  $270^\circ$  is a East heading, and  $360^\circ$  and  $0^\circ$  is a North heading. The heading can be determined by the pilot using known landmarks on the ground. Several instruments can be used to measure the heading. Compasses and flux gate magnetometer use the Earths' magnetic fields to determine the heading with respect to the magnetic North.

**Transformation matrix** A transformation matrix  $\mathbb{T}$  is used to transform a vector or point in one coordinate system to another. The transformation matrix  $\mathbb{T}_{bE}$  transforms the vector in the Earth-fixed frame to the body-fixed frame.

$$\mathbf{v}_b = \mathbb{T}_{bE} \mathbf{v}_E \quad (3-17)$$

with the transformation matrix  $\mathbb{T}_{bE}$  defined as:

$$\mathbb{T}_{bE} = \begin{bmatrix} \cos \psi & \sin \psi & 0 \\ -\sin \psi & \cos \psi & 0 \\ 0 & 0 & 1 \end{bmatrix} \begin{bmatrix} \cos \theta & 0 & -\sin \theta \\ 0 & 1 & 0 \\ \sin \theta & 0 & \cos \theta \end{bmatrix} \begin{bmatrix} 1 & 0 & 0 \\ 0 & \cos \phi & \sin \phi \\ 0 & -\sin \phi & \cos \phi \end{bmatrix} \quad (3-18)$$

$$\mathbb{T}_{bE} = \begin{bmatrix} \cos \psi \cos \theta & \sin \psi \cos \theta & -\sin \theta \\ \sin \phi \sin \theta \cos \psi - \cos \phi \sin \psi & \sin \phi \sin \theta \sin \psi + \cos \phi \cos \psi & \sin \phi \cos \theta \\ \cos \phi \sin \theta \cos \psi + \sin \phi \sin \psi & \cos \phi \sin \theta \sin \psi - \sin \phi \cos \psi & \cos \phi \cos \theta \end{bmatrix} \quad (3-19)$$

The inverse of this matrix can be used to transform a vector from the body-fixed to the Earth-fixed reference frame  $\mathbb{T}_{Eb} = \mathbb{T}_{bE}^{-1}$ .

### 3-3 Doppler Navigation Systems

This section explains how the velocity-range maps of multiple radars can be used to determine the aircraft states required for VFR navigation and attitude determination. This method assumes the VR maps of each radar has been transformed to a single VR pair, this is a single range measurement and a single velocity measurement (Pierrottet et al., 2008).

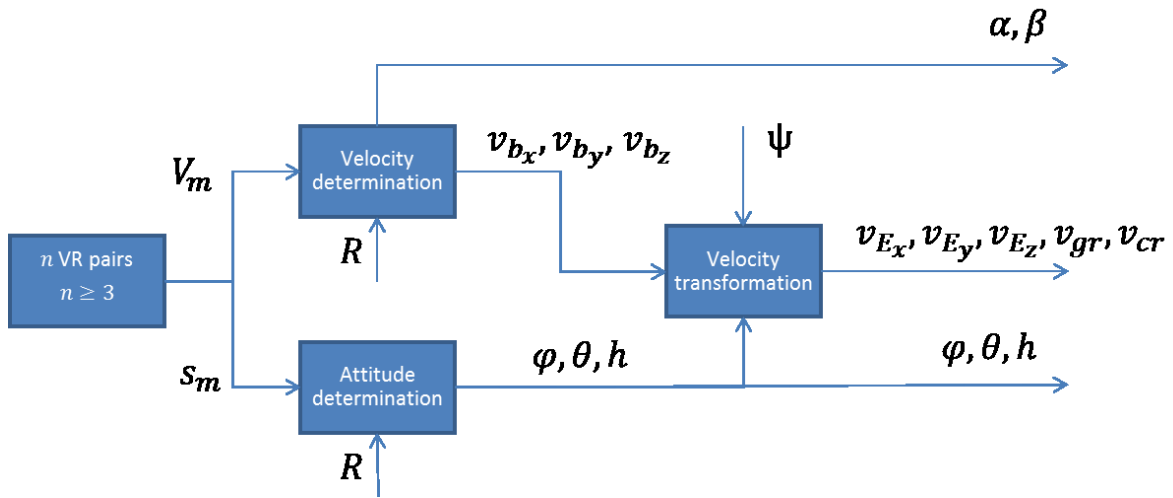


**Figure 3-13:** Schematic representation of the state determination methodology. The range measurements and the antenna orientations are used to determine the height and  $\phi$  and  $\theta$ . The velocity measurements and the antenna orientations are used to calculate  $\mathbf{v}_b$ ,  $\alpha$  and  $\beta$ .  $\mathbf{v}_b$  is transformed to  $\mathbf{v}_E$  using  $\phi, \theta, \psi$ .

On-board radars have been used since the 1950s in civil aviation as Doppler navigation systems to determine the aircraft velocity by measuring the ground velocity (Fried, 1956), and as radio altimeter to determine the aircraft height above the ground. However the weight, complexity and cost of radar systems at the time drove aviation to use other navigation systems and the on-board radars were mostly used by military applications. Improvements in radar technology, miniaturization and computational power have led to an increase in radar applications in the

last couple years (Hyun & Lee, 2009), (Barrenechea, Elferink, & Janssen, 2007). The CAR developed by Selfly ED&A is a relatively small FMCW radar which can be cheaply mounted on almost any part of the fuselage of a small General Aviation aircraft.

A Doppler Navigation System is a system that uses multiple on-board Doppler radars to determine the aircraft velocity and drift angle (Fried, 1964). The Doppler radar, as its name suggests, measures the Doppler shift of the object it is orientated towards. In a DNS the antennas are orientated towards the ground and therefore measure the Doppler shift which is caused by the relative velocity of the aircraft with the ground. As the ground is fixed, the relative radial velocity is a component of the aircraft velocity. Using multiple radars and by comparing the different velocity measurements of each radar, the three dimensional velocity vector of a aircraft can be determined. At least three radars have to be used as the velocity vector of the aircraft has three components.

The radar used in this research is a FMCW radar, which apart from measuring the velocity, can also measure the distance to an object, also referred to as the range measurement. The range measurements of the FMCW radars can therefore be used to determine the aircraft orientation and distance with respect to the earth. The combination of the velocity and range measurements will be used to calculate the aircraft states.

A schematic overview of the state determination methodology is given in Figure 3-13. As can be seen from the Figure, the required inputs are the VR measurements of each radar, the orientation matrix  $R$  of the radars and the heading angle  $\psi$ . The obtained states are: the roll angle  $\phi$ , the pitch angle  $\theta$ , the height Above Ground Level (AGL)  $h$ , the ground speed  $v_{gs}$ , the rate of climb  $v_{cl}$ , the drift angle  $\beta$  and the angle of attack  $\alpha$ .

### 3-3-1 Antenna orientation matrix

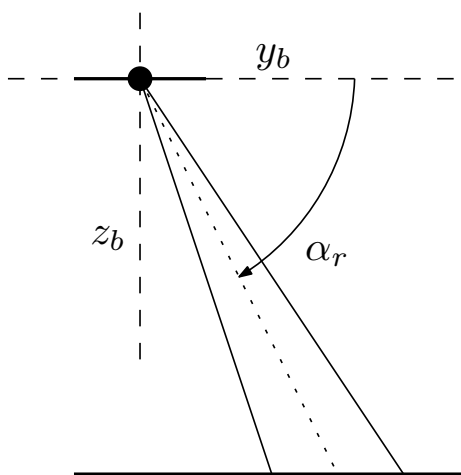


**Figure 3-14:** Definition of the antenna depression angle  $\alpha_r$  in the body-fixed reference frame  $F_b$ .

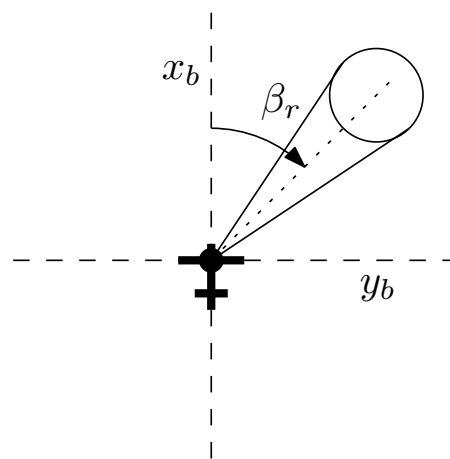


**Figure 3-15:** Definition of the antenna azimuth angle  $\beta_r$  in the body-fixed reference frame  $F_b$ .

A DNS consists of multiple on-board radars. The transmitter and receiver of each radar are considered to use the same antenna to simplify the model. So, the antenna or radar

orientation refers to the orientation of the receivers and the transmitters. Multiple radars can be mounted on the aircraft, each antenna having its own orientation and location on the aircraft. The antenna orientations are represented as unit vectors in  $F_b$ . This unit vector is determined using the depression angle  $\alpha_r$  and the azimuth angle  $\beta_r$ , shown in Figure 3-14 and Figure 3-15 respectively.

Angle  $\alpha_r$  is the angle between the xy-plane and the z-axis ranging from 0 to 90 degrees, with 90 degrees being nadir. Angle  $\beta_r$  is the angle between the xz-plane and the y-axis it goes from 0 to 360 degrees. The unit vector in  $F_b$  that represents the orientation for a single antenna is described as:

$$R = [\cos \alpha_r \cos \beta_r \quad \cos \alpha_r \sin \beta_r \quad \sin \alpha_r] \quad (3-20)$$

### 3-4 Attitude and height determination

The roll angle  $\phi$ , the pitch angle  $\theta$  and the height  $h$  AGL of the aircraft are determined using the range measurements of the on-board radars. The receiver and transmitter are modeled as the same antenna and have a known orientation on the aircraft. First, an example will illustrate how the roll angle  $\phi$  and the height can be computed using two antennas in a 2D situation. This is done to illustrate the geometry of the problem. Following this, the method to determine  $\phi$ , the height and  $\theta$  will be described. Finally, we will look at the case where more than three radars are used.

#### 3-4-1 Two-dimensional example

This example is used to demonstrate the principle to determine the aircraft attitude. The example described in figures above represents the rear view of an aircraft with two on-board radars. In Figure 3-16a the aircraft is in horizontal flight, the two beams are represented as rays and the distance measured by each radar is  $s_1$  and  $s_2$  for radar 1 and 2 respectively.

Figure 3-16b is the same aircraft with a roll angle  $\phi$ . This changes the length of  $s_1$  and  $s_2$  which are then multiplied with the orientation unit vector of the corresponding antenna. This results in the coordinates of two points in  $F_b$ ,  $p_1$  and  $p_2$ . This is shown in Figure 3-16c.

The two points are used to create the normal vector  $\mathbf{n}$  which is normal to the line spanning between  $p_1$  and  $p_2$ . This normal vector is the transformation of a vector along  $z_b$ , with  $\theta = \psi = 0$ .

$$\hat{\mathbf{n}} = \begin{bmatrix} 1 & 0 & 0 \\ 0 & \cos \phi & \sin \phi \\ 0 & -\sin \phi & \cos \phi \end{bmatrix} \begin{bmatrix} 0 \\ 0 \\ 1 \end{bmatrix} \quad (3-21)$$

This gives the expression for  $\mathbf{n}$ :

$$\hat{\mathbf{n}} = \begin{bmatrix} 0 \\ \sin \phi \\ \cos \phi \end{bmatrix} \quad (3-22)$$

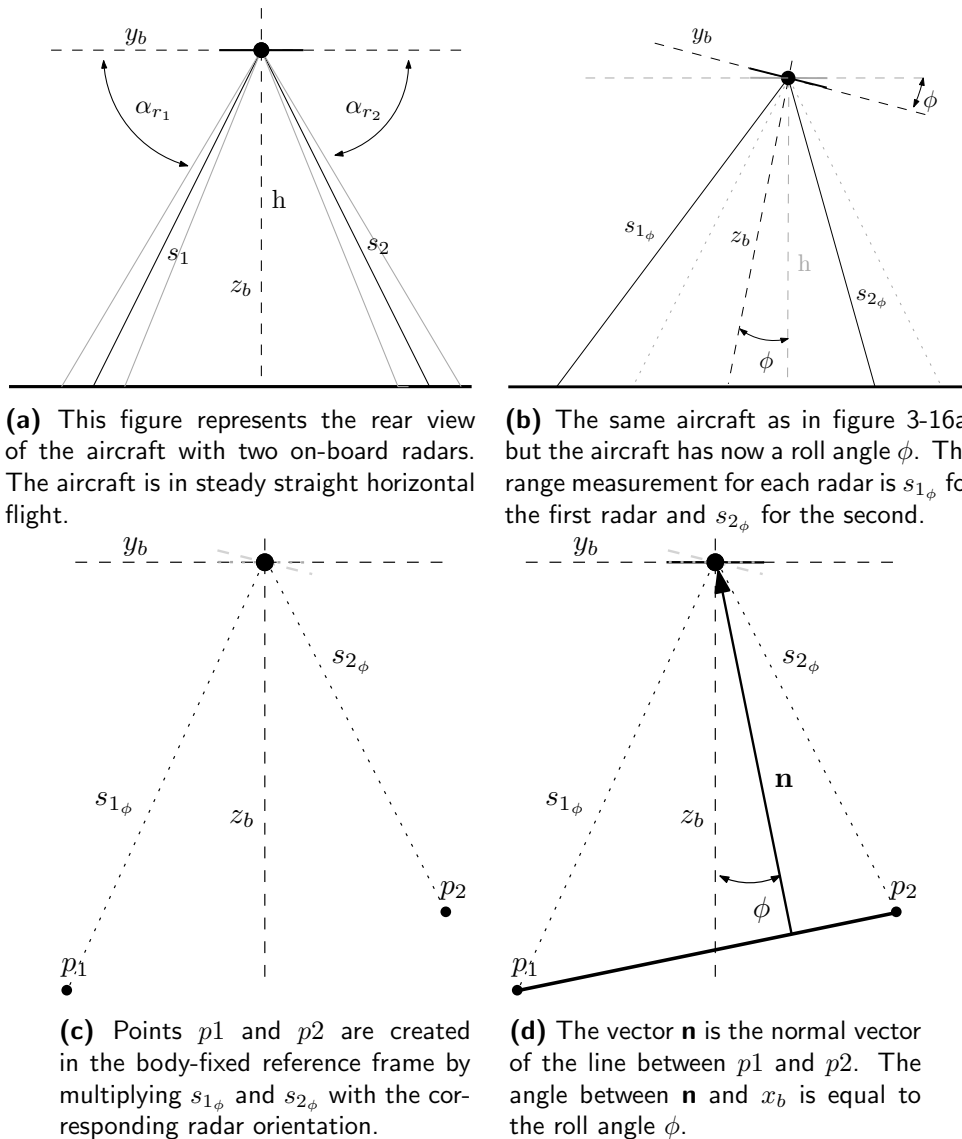


**Figure 3-16:** These figures show the step by step approach to determine the aircraft roll angle and height in a 2D example. Every figure shows the rear view of an aircraft with two on-board radars. The two range measurements are used to create two points and form a line between them. The normal vector of that line is used to calculate the height and roll angle.

From Equation 3-23,  $\phi$  can be calculated:

$$\phi = \arcsin \hat{n}_y \quad (3-23)$$

The points  $p_1$  and  $p_2$  can also be described as vectors in  $F_b$ . The height  $h$  is the projection of one these vector on  $\hat{\mathbf{n}}$ , as shown in 3-24.

$$h = \hat{\mathbf{n}} \cdot \mathbf{p}_1^T \quad (3-24)$$

### 3-4-2 Three-dimensional problem

The example in subsection 3-4-1 serves as illustration to better understand the geometry behind the rotation matrices. Three on board radars are required for the DNS. The Three antennas create a  $3 \times 3$  matrix  $\mathbb{R}$  containing the orientation unit vector of each antenna (Pierrottet, Amzajerdian, Petway, Barnes, & Lockard, 2011).

$$\mathbb{R} = \begin{bmatrix} \cos \alpha_{r_1} \cos \beta_{r_1} & \cos \alpha_{r_1} \sin \beta_{r_1} & \sin \alpha_{r_1} \\ \cos \alpha_{r_2} \cos \beta_{r_2} & \cos \alpha_{r_2} \sin \beta_{r_2} & \sin \alpha_{r_2} \\ \cos \alpha_{r_3} \cos \beta_{r_3} & \cos \alpha_{r_3} \sin \beta_{r_3} & \sin \alpha_{r_3} \end{bmatrix} \quad (3-25)$$

$\mathbf{s}_m$  is a  $3 \times 1$  matrix containing the measured distance of each radar.

$$\mathbf{s}_m = \begin{bmatrix} s_{m_1} \\ s_{m_2} \\ s_{m_3} \end{bmatrix} \quad (3-26)$$

Every unit vector is then multiplied with the corresponding distance measurement creating three points in  $F_b$ .

$$\mathbf{p}_i = [x_b \ y_b \ z_b] = \mathbb{R}_i s_{m_i} \quad (3-27)$$

Now instead of having a line between two points like the example in subsection 3-4-1, there are three points creating a plane. The normal vector  $\mathbf{n}$  has to be defined for the plane that spans between the points. For three points this can be achieved by taking the cross product of the two vectors that span between  $p_1$  and the points  $p_2$  and  $p_3$  respectively.

$$\mathbf{n} = (\mathbf{p}_1 - \mathbf{p}_2) \times (\mathbf{p}_1 - \mathbf{p}_3) \quad (3-28)$$

The orientation of the normal vector can be used to determine the pitch and roll angle because  $\hat{\mathbf{n}}$  is a unit vector along  $z_b$  rotated with  $-\phi$  and  $-\theta$  using the transformation matrix  $\mathbb{T}_{bE}$ .

$$\hat{\mathbf{n}} = \mathbb{T}_{bE} \begin{bmatrix} 0 \\ 0 \\ 1 \end{bmatrix} = \begin{bmatrix} -\sin \theta \\ \sin \phi \cos \theta \\ \cos \phi \cos \theta \end{bmatrix} \quad (3-29)$$

This can be re-written as:

$$\theta = \arcsin \hat{n}_x \quad (3-30)$$

$$\phi = -\arcsin \hat{n}_y \cos \theta \quad (3-31)$$

The projection of any vector, spanning between the aircraft and a point, on  $\hat{\mathbf{n}}$  is the height  $h$  of the aircraft. In Equation 3-32,  $p_1$  is used.

$$h = \hat{\mathbf{n}} \cdot \mathbf{p}_1^T \quad (3-32)$$

### 3-4-3 Plane fitting

The attitude and height determination are performed defining a plane and its normal vector using three points created with the three distance measurements and the orientation matrix. Increasing the number of beams increases the amount of points that have to be fitted on the plane. The equation of a plane is given in Equation 3-33.

$$ax + by + cz + d = 0 \quad (3-33)$$

with the normal vector defined as:

$$\mathbf{n} = [a \ b \ c] \quad (3-34)$$

A least square optimization is used to fit the points on the plane and determine the variables  $a, b, c$ , using the plane of the previous measurement as initial condition.

$$\min S = \sum_{i=1}^n (ax_i + by_i + cz_i + d)^2 \quad (3-35)$$

This yields the normal vector  $\mathbf{n}$  which can be used to determine the aircraft states as explained in section 3-4.

## 3-5 Velocity Determination

The 3D velocity vector of the aircraft in the body-fixed reference frame  $\mathbf{v}_b$ , can be determined using the velocity measures of at least three on board radars  $V_m$  and the orientation matrix  $\mathbb{R}$ . The three measured velocities are combined with the orientation matrix of the antennas resulting in three equations with three unknowns. This system of equations can be solved simultaneously.

$$\mathbb{R} \cdot \mathbf{v}_b^T = \begin{bmatrix} V_{m_1} \\ V_{m_2} \\ V_{m_3} \end{bmatrix} \quad (3-36)$$

with:

$$\mathbf{v}_b = \begin{bmatrix} v_{x_b} \\ v_{y_b} \\ v_{z_b} \end{bmatrix} \quad (3-37)$$

$\mathbf{v}_b$  can be used to determine the angle of attack  $\alpha$  and the side slip angle  $\beta$  of the aircraft.

$$\alpha = \arctan \frac{v_{z_b}}{v_{x_b}} \quad (3-38)$$

$$\beta = \arctan \frac{v_{y_b}}{v_{x_b}} \quad (3-39)$$

The velocity vector in  $F_b$  is then multiplied with the transformation matrix  $\mathbb{T}_{Eb}$  to obtain the velocity vector in  $F_E$ . The transformation matrix is created using  $\phi$ ,  $\theta$  and  $\psi$ . The angles  $\phi$  and  $\theta$  are obtained in Equation 3-31 and 3-30 respectively. As angle  $\psi$  cannot be determined with the DNS, this angle has to be imported from an external source.

$$\mathbf{v}_E = \mathbb{T}_{Eb} \mathbf{v}_b \quad (3-40)$$

The rate of climb  $v_{cl}$  of the aircraft is the vertical component of  $\mathbf{v}_E$

$$v_{cl} = -v_{z_E} \quad (3-41)$$

The ground speed  $v_{gr}$  of the aircraft is calculated with the sum of both horizontal components of  $\mathbf{v}_E$ .

$$v_{gr} = \sqrt{v_{x_E}^2 + v_{y_E}^2} \quad (3-42)$$

### 3-5-1 Overdetermined system

The number of rows is equal to the number of radars in the DNS, therefore the system described in Equation 3-36 becomes overdetermined with more than three radars.

$$\mathbb{R} \cdot \mathbf{v}_b^T = \mathbf{V}_m \quad (3-43)$$

$\mathbf{v}_b$  is found using the least square minimization method. The solution of  $\mathbf{v}_b$  minimizes Equation 3-44. In this equation  $\mathbf{V}_m$  is a  $n \times 1$  matrix and  $\mathbb{R}$  a  $n \times 3$  matrix, with  $n =$  the number of radars.

$$\|\mathbf{V}_m - \mathbb{R} \cdot \mathbf{v}_b^T\|^2 \quad (3-44)$$



---

# Chapter 4

---

## Problem Statement

This chapter defines the problem statement of the thesis. Section 4-1 first describes which states are required for navigation and attitude determination in VFR flight. Sections 4-2, 4-3 and 4-4 describe the problems faced using the state derivation method with the CAR. Section 4-6 summarizes everything in a single research question.

### 4-1 Navigation and Attitude Determination

Flying VFR has the benefits of independent flight, but is constrained to flying to VMC. The pilot has to perform the three tasks of CA, navigation, and attitude determination visually. Without visibility the aircraft is blind and cannot fly safely. Selfy ED&A has developed the FMCW CAR which is able to detect the ground and other airborne targets. This application could be used to support the pilot in the CA tasks so VFR flight can be performed under non-VFR conditions. The two other tasks of navigation and attitude determination are the subject of this thesis.

In order to determine the performance of a DNS, the accuracy, to which the required aircraft states for navigation and attitude determination can be determined, is quantified. These aircraft states are:

- Roll angle  $\phi$
- Pitch angle  $\theta$
- Heading angle  $\psi$

The aircraft states required for navigation are:

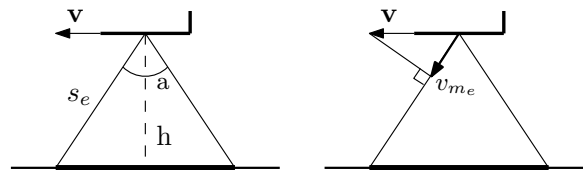
- Latitude  $\Phi$
- Longitude  $\lambda$

- Elevation or height  $h$
- Ground speed  $v_g$
- Heading angle  $\psi$

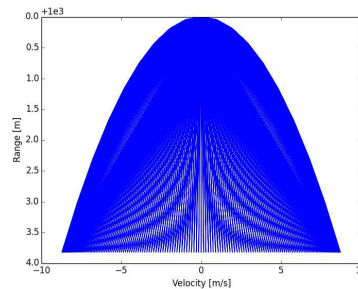
The accuracy of the obtained states can be compared to the pilots ability to navigate and determine the attitude visually. The attitude of the aircraft is a direct measurement of  $\phi$ ,  $\theta$  and  $\psi$ , while navigation consists of a horizontal and vertical position. The horizontal position is determined by integrating the ground speed over a period of time and the vertical position is directly determined with the height measurement.

The method used to calculate the aircraft states in section 3-3 does not calculate the aircraft heading, which is an important state, because it is required for dead-reckoning navigation and it is one of the Euler angles which describes the aircraft attitude and transforms the velocity vector from  $F_b$  to a vector in  $F_E$ . Therefore, angle  $\psi$  has to be obtained with another sensor, such as a flux-gate magnetometer.

## 4-2 Beam Width



(a) Aircraft with a single radar with aperture  $a = 10^\circ$ .



(b) The VR map of a radar oriented towards nadir.

**Figure 4-1:** Example of an aircraft flying at  $100\text{m/s}$  at a height of  $1000\text{m}$  with a single radar oriented towards nadir. The beam projection on the ground is a perfect circle and is segmented in  $n \times n$  points. The relative radial velocity and range of each point with respect to the aircraft is calculated and represented in Figure 4-1b.

Unlike other DNS systems that operate with an aperture angle smaller than  $5^\circ$  (Fried, 1956), the CAR has a relatively large aperture angle of  $10^\circ$ . This is because it is not a radar designed for Doppler navigation, but for CA. The large aperture angle results in a large beam width and therefore a large area of ground covered by the beam for every measurement. The ground covered by the beam is minimum when the radar is oriented towards nadir. It can

be approximated by the surface of a circle with a radius that is proportional to the aircraft height AGL. At a height of  $1000m$  this is a radius of  $87m$  and a surface of  $24047m^2$ .

$$surface = \pi r^2 = \pi \left[ h \tan \frac{a}{2} \right]^2 \quad (4-1)$$

Where  $a$  is the aperture angle. This only holds for a horizontal aircraft with a radar oriented towards nadir ( $\alpha_r = 90^\circ$ ).

The radar image will therefore not see the ground as a single velocity and range measurement, but a clutter of points with ranges and velocities corresponding to all the combinations that can be measured on this surface. Figure 4-1a shows a single radar with an aperture of  $a$  oriented towards nadir. On the left image, the difference between the range measured with a single radar due to its beam width is made clear. The range measurements vary between  $s = h$  and  $s_e = h \cos \frac{a}{2}$ . Where  $s$  corresponds to the distance to the ground right underneath the radar, and  $s_e$  to the ground at the extremities of the beam. The same holds for the measured velocity, and this is depicted in the right image. The measured velocity is the projection of the velocity vector of the aircraft on the orientation vector of the radar. For an aircraft flying steady horizontal flight, the relative radial velocity of the ground exactly under the aircraft is  $0m/s$ . At the extremities of the beam the relative radial velocity is equal to  $0.087v$ , and  $-0.087v$  for the aft looking portion of the beam. The velocity and range of the ground which is in the radar beam are plotted in a VR map. This models the ground as a  $m \times m$  grid where each grid point has its own VR pair.

As can be seen from Figure 4-1 the processed radar image contains a whole clutter of points, instead of a single velocity and range measurement per radar. However, the method to determine the aircraft states, requires a single VR pair. Therefore, to transform the spectrum of the ground clutter into a single VR pair, the average is taken on both the range and the velocity. The downside of this method is that it is sensitive to noise, and if the beam projection on the ground is not a perfect circle, but a slanted ellipse for example, this average will not be the center of the radar beam, but the center of the ground projection. The center of the ground projection is only the center of the beam when the ground projection is symmetric. This is only the case when the beam is oriented towards nadir.

### 4-3 Terrain Ambiguity

Variations in terrain height cause an ambiguity to arise because this can be interpreted as a roll or pitch angle of the aircraft. This means the DNS performance will be dependent on the terrain below it. The pitch angle, roll angle and height of the aircraft are calculated using the range measurements of the radars. When rolling to the right, the range measured by a right-side oriented radar will be smaller than the range measured by the left-side oriented radar. This difference is used to determine that the aircraft is rolling. However, when flying over non-flat terrain, the range measurements of the radars will also show differences, this while the aircraft is flying straight horizontal flight. It is therefore impossible to determine a difference in terrain from a roll or pitch angle. This is depicted in a 2D example in Figure 4-2. In this example the range measurements  $s_1 = s_{1\phi}$  and  $s_2 = s_{2\phi}$ , however the roll angle of the aircraft is not the same. In this way, the range measurements directly affect the height, roll

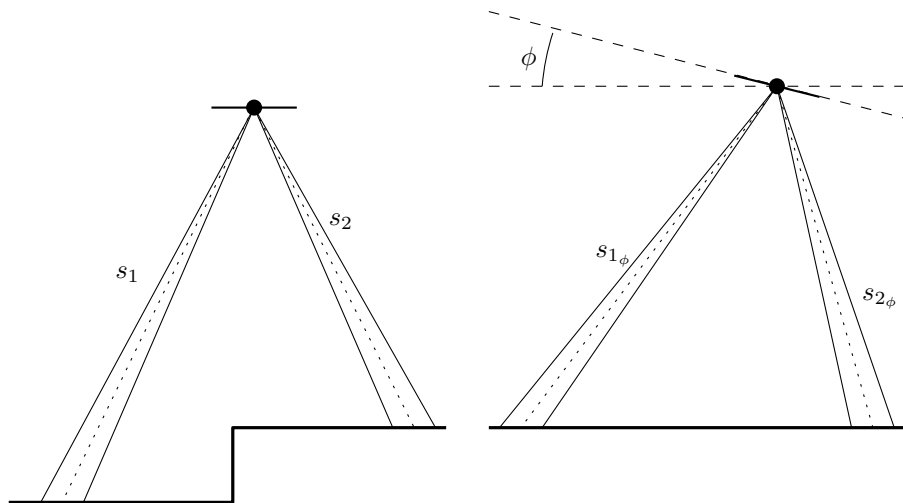


**Figure 4-2:** Example of the ambiguity that can occur when flying on non-flat terrain. In both situations the radars measure the same distance  $s_1 = s_{1\phi}$  and  $s_2 = s_{2\phi}$ . This illustrates that this system cannot see the difference between the two situations and the DNS will determine the aircraft has a roll angle  $\phi$  in both cases.

angle and pitch angle. Other parameters such as ground speed, and climb rate are indirectly affected because they are calculated using pitch and roll.

#### 4-4 Radar Configuration

The CAR developed by Selfly ED&A is light weight, small and can be fitted almost everywhere on the aircraft. It can also be oriented in any direction. This permits the placement of multiple radars on the aircraft. From DNS theory it has been determined that at least three radars have to be used in Janus configuration and that each radar should be oriented towards the ground at all time. There is theoretically no maximum amount of radars for the DNS. The only limitation is set by the aircraft structural capacity. The thesis will therefore research what the ideal configuration and number of on-board radars is to determine the aircraft states.

#### 4-5 Python model

The Doppler Navigation System model should be created such that it can have data from the flight computer and radar data as input so that it can be used to determine the aircraft states during a flight. When not used in a flight, the model should be able to model the radar data using flight data, terrain elevation maps and radar parameters.

#### 4-6 Research Question

The goal of this thesis is to determine if a DNS with on-board CARs designed by Selfly ED&A can support the pilot in VFR flight when weather conditions are degraded.

The accuracy of the aircraft states required for aircraft navigation and attitude determination will therefore be quantified. Flight tests using real on board FMCW radars are expensive and time consuming, therefore a model of the FMCW DNS will be created in Python and flight data from flight simulators will be used instead of flight data from a real flight.

The research question can therefore be summarized as follow:

*Can aircraft states required for VFR navigation and attitude determination be derived using a DNS model based on the radar developed by Selfly ED&A CAR, and can this model be used to identify the antenna configuration optimizing the navigation performance?*



---

## Chapter 5

---

# Simulator in Python

As described before, a Doppler Navigation System consists of multiple on-board radars. Each radar generates its own signal which is mixed with a received signal to form the beat signal. Every beat signal is processed resulting in separate VR data for each on-board radar. This data is reduced to a single VR pair per radar. The VR pairs and the antenna orientations are then used to calculate the aircraft states. The schematic representation of the data flow in a DNS is given in Figure 5-1. The goal of this thesis is to model a DNS in Python. The

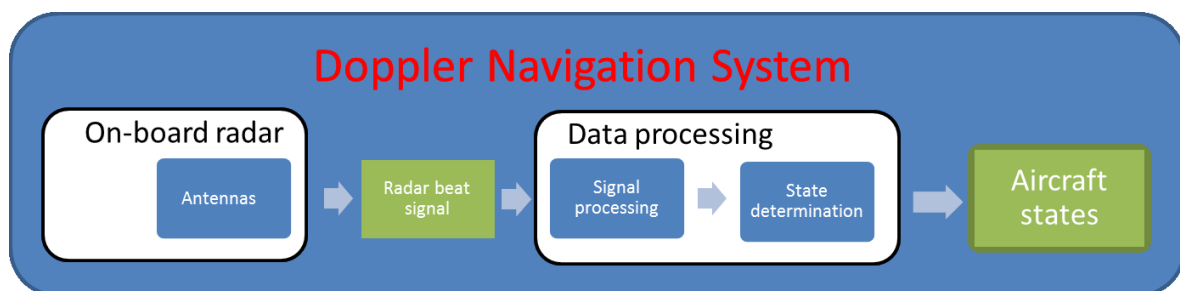


**Figure 5-1:** Schematic representation of the data processing of a DNS

schematic representation of the complete model is shown in Figure 5-2. The Data Acquisition module generates flight data using a flight simulator. It is important to notice that it is decoupled from the DNS model. The DNS does not work online but performs a simulation of a flight using flight data of an already performed flight or simulated flight. This flight data is used as input for the DNS model. The DNS model consists of a FMCW Radar Model module and a Data Processing module. The FMCW Radar Model module creates each radar of the DNS model and generates the beat signal of each radar. The Data Processing module processes the beat signal of each radar and calculates the aircraft states.

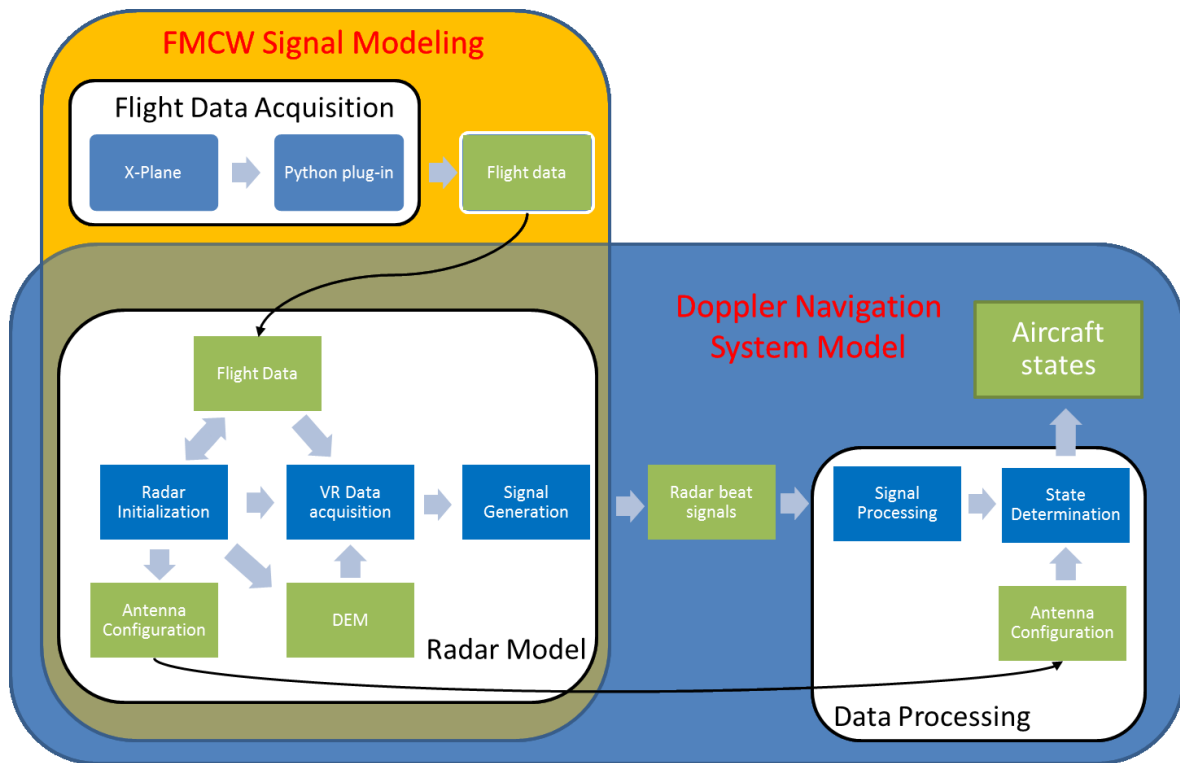


**Figure 5-2:** Schematic overview of the main components of the Doppler Navigation System model.

## 5-1 Flight Data Acquisition

The flight data acquisition module is a tool developed to generate flight data for this research using the flight simulator X-Plane. This tool allows the user to simulate a flight in X-Plane and to save the aircraft states as a .npz file. This is completely decoupled from the DNS model. The advantages of such a tool is that the user can choose the weather conditions of the flight, the flight path being flown, and specific maneuvers can be performed during the flight. Once the user has performed a flight in X-Plane, the saved flight data can easily be used for a simulation of the DNS model. This separation between flight data acquisition and DNS model gives two main advantages:

- The user can use the same flight data with different DNS model parameters, thus seeing the individual effects of each parameter on the accuracy of the states.
- The user can create their own flight data, changing weather settings and making specific flight maneuvers to see the effect these have individually on the performance of the radar model.

The main disadvantage is that the states are not calculated in real time, therefore this model cannot be used while flying. Next versions of this model could be made to function online and combined to displays indicating the aircraft states while flying.

**Table 5-1:** Aircraft states retrieved from the flight simulator with the python plug-in

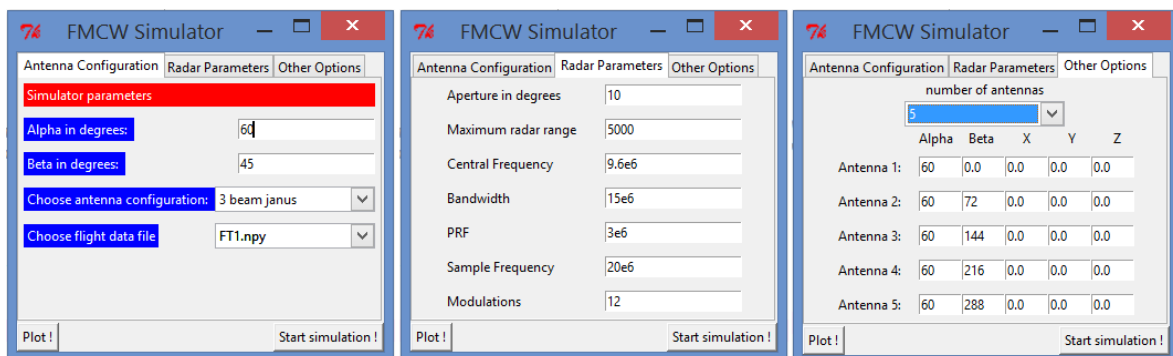
Aircraft states	Unit	Description
Latitude	$^{\circ}$	The aircraft latitude
Longitude	$^{\circ}$	The aircraft longitude
Elevation	$m$	Elevation above Mean Sea Level
$\phi, \theta, \psi$	$^{\circ}$	Roll, Pitch and Heading angle
$v_{x_{OGL}}, v_{y_{OGL}}, v_{z_{OGL}}$	$m/s$	Velocity components in the Open GL reference frame
$\alpha, \beta$	$^{\circ}$	Angle of attack and side slip angle

The version of X-Plane used in this research is X-plane 9, and the python plug-in is also compatible with X-plane 10. X-Plane is a very realistic flight simulator which models the aircraft flight dynamics. The aircraft states are stored as so called 'Datarefs' in X-Plane, and can be accessed by the plug-in. The states being read by the Python plug-in are summarized in Table 5-1. The update rate of these states can be chosen by the user, and is set at 1 Hz.

## 5-2 Doppler Navigation System Model

The simulations are controlled by a Graphical User Interface (GUI), which opens when the program is launched. This GUI enables the user to input the DNS model parameters such as the number of radars, their orientation, position, and signal type. The user also selects the flight data that will be used in the simulation. The first action carried out by the DNS is the radar initialization. This module creates multiple radars in the DNS model, and loads the flight data and the correct Digital Elevation Map (DEM). After the initialization a loop iterates through the flight data, calculating the aircraft states at every iteration. This iteration stops when all the flight data has been processed. When the simulation is finished the user can decide to plot the results.

### 5-2-1 Graphical user interface

**Figure 5-3:** An overview of the GUI's three tabs

The GUI allows the user to input the parameters for the simulation. The GUI is represented in Figure 5-3 and is a window containing three tabs. The three tabs are presented next to

**Table 5-2:** Radar parameters

Radar parameters	Unit	Description
$f_c$	Hz	Central frequency
B	Hz	Bandwidth of the frequency modulation
PRF	Hz	Pulse Repeat Frequency
$f_s$	Hz	Sample frequency
K	-	Number of modulation per measurement
$R_{max}$	m	Maximum radar range
$a$	°	Aperture angle

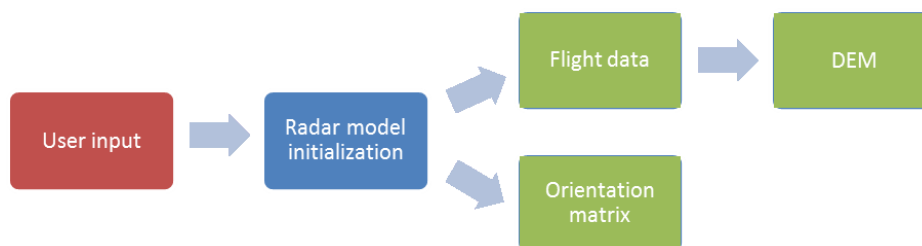
each other in the Figure. There are three main inputs for the simulation: the antenna/radar configuration, the flight data used for the simulation, and the radar parameters

**Antenna/radar configuration** The user can decide how many on-board radars are used and manually input their orientation and position on the aircraft. The user can also choose a predefined configuration that only requires the user to set the angles alpha and beta.

**Flight data** The user can select a .npz file that will be used in the simulation. This can be a file created using the flight data acquisition module or any other flight data as long as it has the right format.

**Radar parameters** The user has to set the radar parameters which have default values corresponding to the characteristics of the CAR. The radar parameters and their units are listed in Table 5-2. These parameters are used in the signal generation and signal processing module.

### 5-2-2 Radar initialization module

**Figure 5-4:** Outputs of the radar initialization module

The radar initialization module initializes the simulation. The first action is to process the user inputs. The radar parameters of all the radars of the DNS model are set. The orientation of each antenna is stored in the orientation matrix which is used later to determine the states. Then, the selected flight data is loaded into the model. The aircraft geographic location is read from the selected flight data to determine what DEM will be used in the simulation. A brief summary of the main actions of the initialization module is given below:

1. Create orientation matrix  $\mathbb{R}$
2. Load flight data file
3. Load DEM file
4. Start simulation

At the end of the initialization the simulation of the flight is started. The flight data is read in chronological order, and the aircraft states are calculated for each iteration.

### 5-2-3 Velocity-range data acquisition module

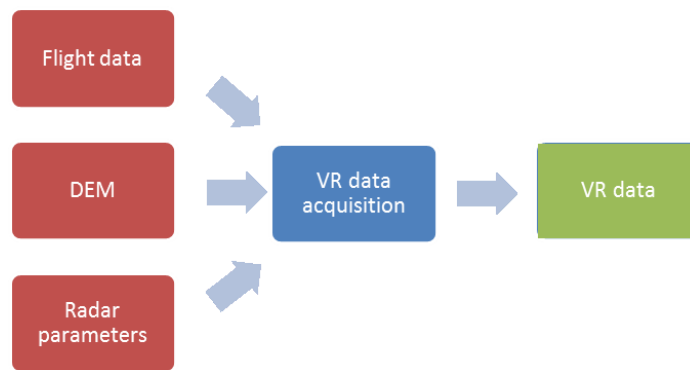


**Figure 5-5:** Schematic representation of the inputs and outputs of the VR data acquisition

The frequency of the beat signal generated by a target in the radar beam is a function of the velocity and range of that target. In a DNS the radars are oriented towards the ground, thus the relative radial velocity and range of the ground with respect to each antenna have to be calculated to create the beat signal. Only once this VR data is acquired, can the beat signal be generated.

This module calculates the VR data for each radar separately. First it determines what part of the ground is within the beam of a radar using: the antenna orientation on the aircraft, the aircraft orientation with respect to the earth, the aperture angle of the antenna, and the terrain height from the DEM. Then, if the ground is also within the range of the radar, the ground is modeled as a grid of points, and for each point on that grid, the relative radial velocity and the range with respect to the radar is calculated. Each ground grid point in the beam returns a VR pair, and all the VR pairs of a radar are referred to as the radar VR data. A schematic overview of the major inputs and outputs of this module is represented in Figure 5-5.

$$d = \sqrt{(x_g - x_a)^2 + (y_g - y_a)^2 + (z_g - z_a)^2} \quad (5-1)$$

The relative velocity is the projection of the velocity vector of the aircraft on the unit vector of the vector spanning between the aircraft and that point on the ground.

$$\mathbf{v}_r = \frac{(x_g - x_a) v_{x_E} + (y_g - y_a) v_{y_E} + (z_g - z_a) v_{z_E}}{d} \quad (5-2)$$

This returns an array containing VR data of each radar.

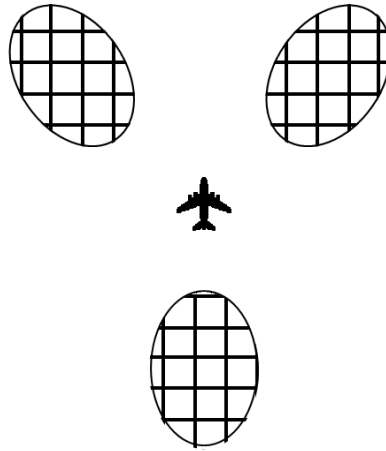


**Figure 5-6:** The ground projections of three radars is segmented in grids of  $n \times n$  points. The relative velocity and distance of each point to the aircraft is calculated creating a VR pair for each point.

#### 5-2-4 Signal generation module

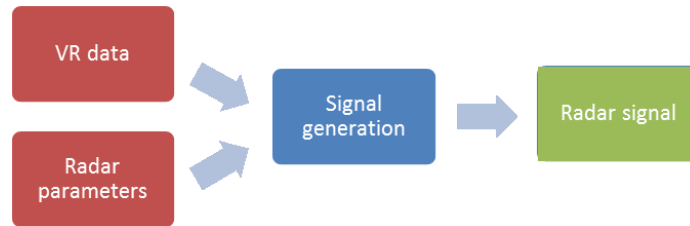


**Figure 5-7:** Inputs and outputs of the signal generation module

This module generates the beat signal of each radar. As explained in Chapter 3 the phase of the beat signal can be approximated with the Equation 5-3.

$$\Phi_b = 2\pi \left[ \tau_0 f_c + k f_d T + \left( f_d + \frac{B}{T} \tau \right) t_k \right] \quad (5-3)$$

In Equation 5-3, the variables are  $f_d$ ,  $\tau$ , and the radar parameters  $f_c$ ,  $k$ ,  $T$ ,  $B$ . With  $f_d$  as a function of velocity  $v$ , and  $\tau$  a function of range  $s$ . The radar parameters have been set in the radar initialization and the VR data has been calculated in the VR data acquisition module. Each VR pair creates its own beat signal and all the signals of a VR data set are added up to form the beat signal  $x_b$  of the radar.

$$x_b = \sum_{n=0}^{N-1} \sin \Phi(v_n, s_n) \quad (5-4)$$

where  $N$  is the number of VR pairs.

The signal generation module is too computationally intensive to be used in the DNS model. Creating one VR map with relatively few VR pairs takes 60 hours on a normal laptop. Therefore, this module has been left out and the assumption is made that the transformation of a signal to VR map and VR pair is perfect. The ground reflectivity and the effect of distance on the amplitudes of the signals are not modeled in the signal generation module however this can easily be implemented in the existing framework. The signal generation module is only required for the model which has to generate its own VR map and signal. Therefore, the signal processing and state derivation modules have been designed to function independently with multiple beat signals as input.

### 5-2-5 Signal processing module

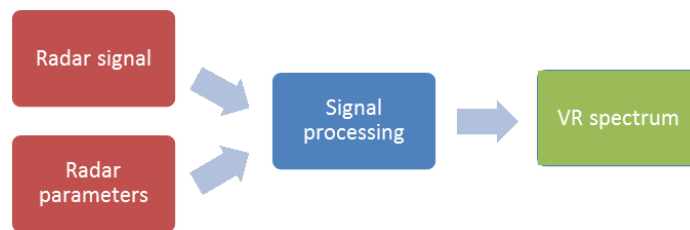


**Figure 5-8:** Inputs and outputs of the signal processing module

This module transforms the beat signal of a radar into a single VR pair, using the radar parameters. The signal processing is done with a two dimensional Fourier transformation according to the method described in Chapter 3. This creates a two dimensional spectrum with peaks at the VR pairs of the VR data set as shown in Figure 5-9a. This spectrum is averaged to a single VR pair. A DNS system consists of multiple radars, and this is done for every radar individually, resulting in a VR pair per radar.

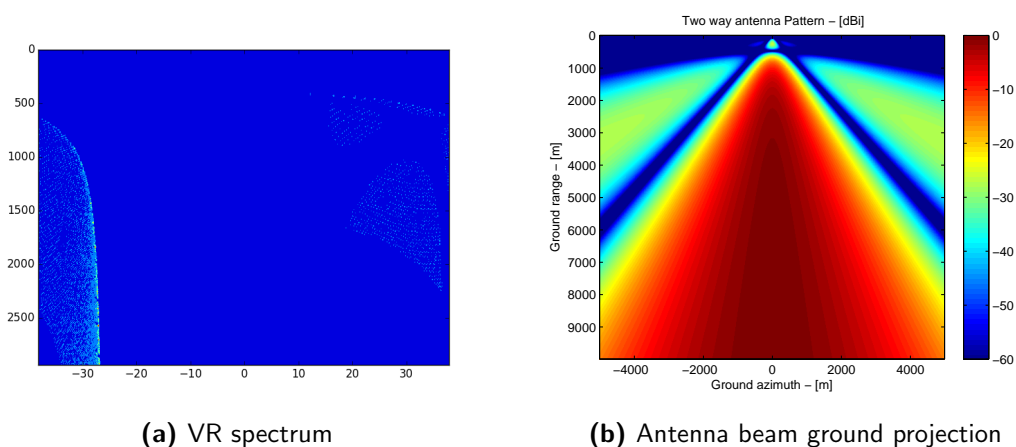


**Figure 5-9:** On the left, the velocity-range spectrum modeled with Python. The antenna beam ground projection is represented on the right. The aircraft flies horizontally with a velocity of  $50m/s$ . The spectrum is generated by creating a beat signal with the VR data of the ground. Then the signal is processed to the VR spectrum. Due to the Doppler ambiguity the ground clutter is shifted in the spectrum.

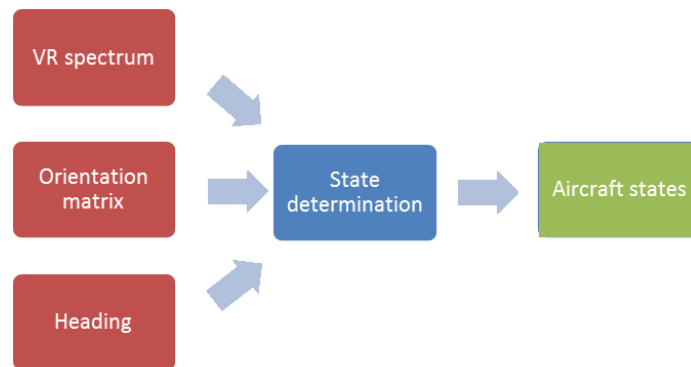
**Table 5-3:** Radar parameter settings used to model and process the signal.

Radar parameters	Value
$f_c$	9.6 GHz
B	15 MHz
PRF	4.9 kHz
$f_s$	10 MHz
K	1022
$R_{max}$	5000m
$a$	10°

Figure 5-9a shows the modeled VR spectrum for an aircraft flying at 50m/s straight horizontal flight. The radar ground projection is shown in Figure 5-9b. The signal generation module was too computational intensive, this module was also left out of the final model. This VR map was used as example to verify the signal generation and processing module. The model can easily be adapted to process a signal from a real radar, skipping the signal generation module. However, there is no available data from a real radar with the right orientation.

This model uses the following radar parameters:

### 5-2-6 State derivation module

**Figure 5-10:** Inputs and outputs of the state determination module

This module uses the VR pairs of each antenna and their orientations to determine the aircraft states. The antenna orientation is determined by the user at the radar initialization and the VR pairs are extracted from the signals in the Signal Processing module. The states are derived according to the methodology described in Chapter 3. The height AGL, and the angles  $\phi$  and  $\theta$  are computed using the range measurements. The velocity measurements are used to calculate the velocity vector of the aircraft in the body-fixed reference frame  $F_b$ . The velocity vector is transformed to the Earth-fixed reference frame  $F_E$  using the obtained  $\phi$  and  $\theta$ , and  $\psi$  from the flight data. The velocity vector in  $F_b$  is also used to calculate  $\alpha$  and  $\beta$ .

## 5-3 Digital Elevation Map

A DEM is a file containing terrain elevation data for the geographical coordinates latitude  $\Phi$  and longitude  $\lambda$ . The largest collection of DEMs is the Shuttle Radar Topography Mission (STRM) database, which covers most of the world. The elevation data is stored in files that cover a surface of 1 degree longitude by 1 degree latitude. When the simulator is initiated, the first  $\Phi$  and  $\lambda$  values are used to create a two dimensional DEM array. This is done only once to save computational power during the simulation, however it constrains the flight not to exceed the DEM area. To find the elevation of any x,y coordinates in  $F_E$  the x and y coordinates are transformed to latitude and longitude coordinates using the geographical coordinates of the aircraft.

$$\Phi = \Phi_{aircraft} + \frac{x}{R_{Earth}} \quad (5-5)$$

$$\lambda = \lambda_{aircraft} + \frac{y \cos \Phi}{R_{Earth}} \quad (5-6)$$

DEM files have an accuracy of 3 arc seconds meaning the DEM is an array of 1201 x 1201 height values. To read the height value knowing (x,y) of a random point in  $F_E$ , the geographical coordinates are calculated using equations 5-5 and 5-6. These coordinates are converted to indexes of the two dimensional array containing the terrain height. An example of the DEMs is shown in Figure 5-11.

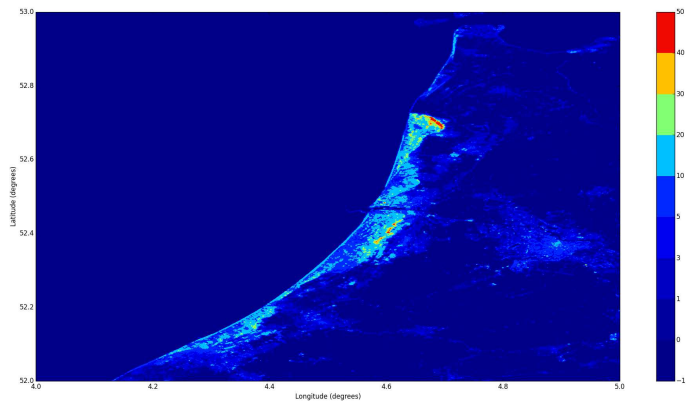


**Figure 5-11:** This is a DEM of the area between  $4^\circ$  and  $5^\circ$  longitude and  $52^\circ$  and  $53^\circ$  latitude. The DEM has an accuracy of 3 arcsecond. Every pixel is an area of  $3''$  which is approximately  $100mm$ .



---

# Chapter 6

---

## Results

The simulations of the DNS were performed using three sets of data: FD1, FD2 and FD3. The trajectory of the aircraft for each data set is shown in Appendix A. The DEM used is a 3arc seconds STRM of  $1^\circ \times 1^\circ$  ranging between  $4^\circ$  and  $5^\circ$  longitude, and  $52^\circ$  and  $53^\circ$  latitude. The DNS model parameters such as the radar configuration, the radar aperture angle, the Digital Elevation Map, and the flight data set were varied for the different experiments.

### 6-1 Flight Data

Flight data was acquired using the flight simulator X-Plane 9. The simulated flights are all performed in the area between  $52^\circ$  and  $53^\circ$  latitude, and  $4^\circ$  and  $5^\circ$  longitude to stay in the range of the DEM. This area contains a large area of the north sea, most of the dutch coast, as well as Schiphol airport. There is a great diversity of landscape, the sea is a flat terrain and the dunes vary in height between 0 and 50 meters. The sea is assumed to have no velocity and there is no wind.

### 6-2 Radar Configuration

The radar configuration is the combination of all the antennas of the receivers and transmitters on the aircraft. An antenna is considered both a transmitter and receiver in the model. As stated earlier, three antennas are required to solve the system of equations to obtain a good estimate of the aircraft states. However, more than three antennas can be modeled and each orientation can vary, meaning there are many radar combinations possible.

#### 6-2-1 Individual antenna orientation

Each antenna has two angles which describe its angular orientation with respect to the aircraft body-fixed reference frame  $F_b$ . The depression angle  $\alpha_r$  and the azimuth angle  $\beta_r$ , as shown

in Figure 3-14 and 3-15. Angle  $\alpha_r$  ranges between  $0^\circ - 90^\circ$ .  $\alpha_r = 0^\circ$  means the antenna is oriented along the  $xy$  - plane of  $F_b$ . For  $\alpha_r = 90^\circ$ , the beam is oriented towards nadir. Angle  $\beta_r$  is defined similarly as the heading of the aircraft. It ranges from  $0^\circ - 360^\circ$  in the  $xy$  - plane in  $F_b$ . Each antenna can therefore be oriented in  $F_b$  using these two angles.

### 6-2-2 Standard radar configuration

Some standard configurations have been created allowing the user to only have to input two variables for each simulations. These are configurations J3, J4, T3 and T4, shown in Figure 6-1. The user only has to input one angle  $\alpha_r$  and one angle  $\beta_r$  to create one of these configurations.

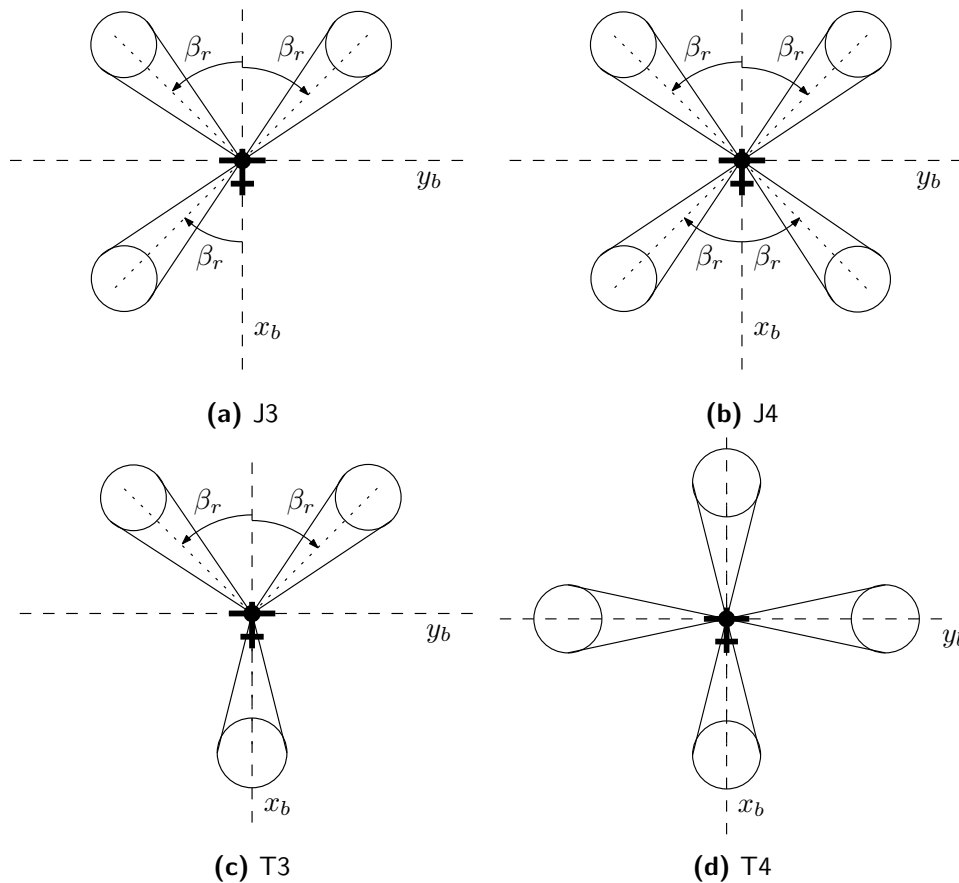


**Figure 6-1:** These figure show the top view of standard configurations used in this thesis and defined in the model. These configurations allow the user to only set one  $\alpha_r$  and one  $\beta_r$  to obtain a configuration, as opposed to setting the  $\alpha_r$  and  $\beta_r$  of each separate radar.

## 6-3 Graph Explanation

The results of the state determination are plotted using two subplots per state. The upper subplot contains the value of the state over time expressed in degree, meter, or meter per

second, depending on the state. The red line in the upper subplot is the reference which is directly read from the flight data. The other lines are the states calculated using DNSs. Multiple lines means multiple DNS configurations are being represented.

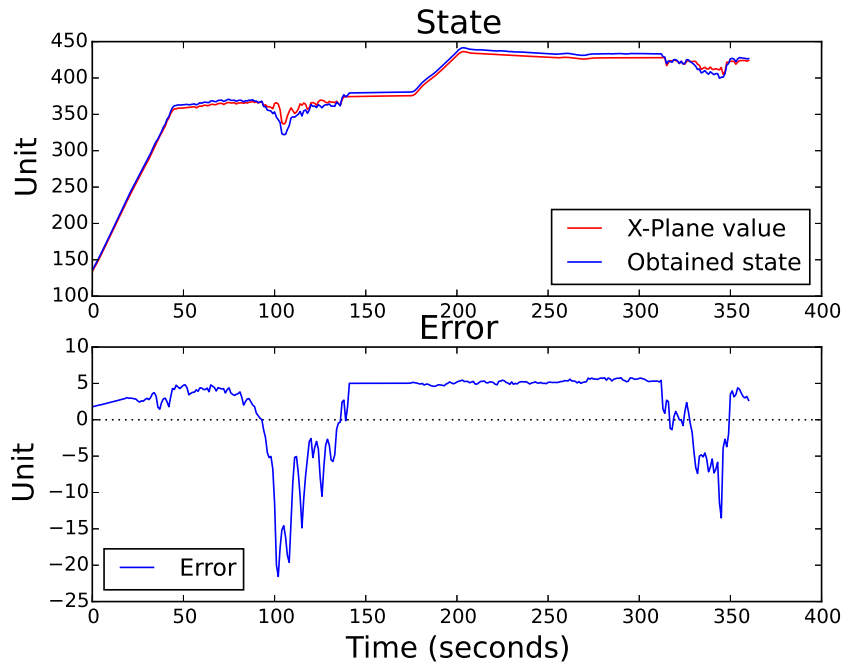


**Figure 6-2:** This figure shows the format in which the results are presented. The top plot shows the obtained state and the state from the flight data. The bottom plot shows the error between the two.

The lower subplot shows the difference between the reference state and the calculated state. The error is calculated as follow:

$$\epsilon = x_{fd} - x_{obt} \quad (6-1)$$

With,  $\epsilon$ : the error.

$x_{fd}$ : the reference state from the flight data.

$x_{obt}$ : the obtained state from the DNS

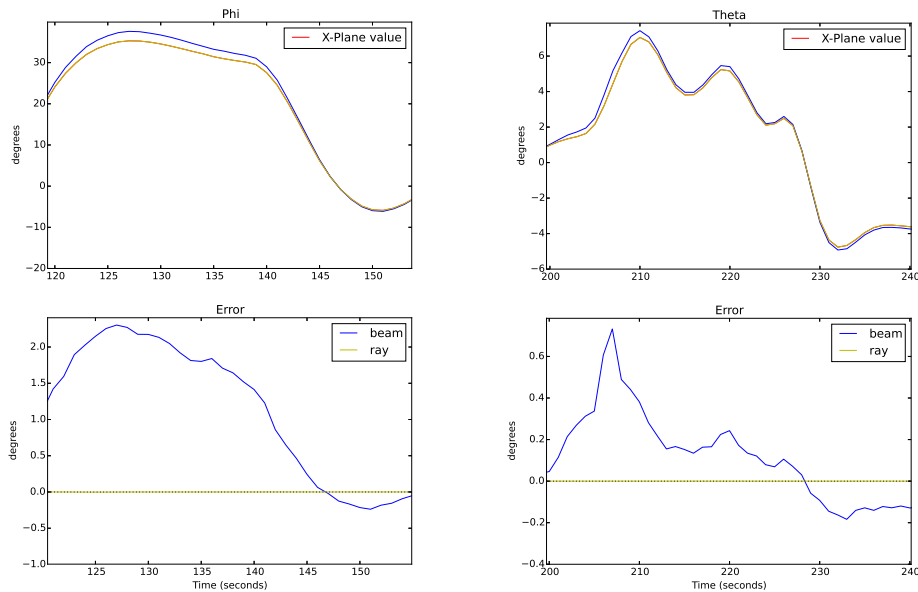
The vertical axis shows the error in the same unit as the subplot above. Each line in the upper subplot has an error line of the same color in the lower subplot.

## 6-4 Effect of Beam Width

One of the problems stated in Chapter 4 is the fact that this CAR has an aperture angle of  $10^\circ$ , which negatively affects the state accuracies due to the averaging of the ground clutter. This effect induces an error in the VR pair which in turn results in an error in the states. This effect is demonstrated assuming a flat earth to prevent any effect due to non-flat terrain. The Figure B-1 shows the effect of a large beam width compared to a small beam width for

the height, roll angle and pitch angle. The beam has an aperture of  $10^\circ$  and is represented as 'beam', while the ray an aperture angle of  $0^\circ$  and is represented as 'ray' in the graph. The Root Mean Square (RMS) errors, the maximum and minimum errors of the states for the 'beam' configuration are shown in table 6-1. The ray configuration has no error except for the rate of climb.

Figure 6-3a and Figure 6-3b illustrate the effect of the beam width on the accuracy of  $\phi$  and  $\theta$  respectively. These three states are all functions of the range measurements. As can be seen from the results, the ray DNS has no error while the beam DNS shows maximum height error of  $13.65m$ , the maximum roll and pitch errors are  $2.42^\circ$  and  $0.44^\circ$ . It can be concluded that the aperture of  $10^\circ$  results in an error in these states which is proportional to the state itself. To show this correlation, the error is plotted against the state in Figure 6-4.



(a) Roll angle during a roll

(b) Pitch angle during a pitch up

**Figure 6-3:** The effect of the beam width on the error of the states  $\phi$  and  $\theta$ . This figure shows the obtained  $\phi$  and  $\theta$  and their error for a part of two simulation with FD 2. The radar configurations in both simulations is J4, with  $\alpha_r = 40^\circ$  and  $\beta_r = 45^\circ$ . The aperture angle has the values  $10^\circ$  for the beam and  $> 1^\circ$  for the ray.

The other states and their errors are plotted in Figure B-1 in appendix A. The error of the states is due to averaging the measured range value of the radars. As  $\phi$ ,  $\theta$  and  $h$  increase, the ground projections become asymmetric ellipses. The average range of one radar measurement is therefore not the range measured with a ray which is the center of the beam, but the average of all the range values. This average is slightly larger than the ray value do to the elongation of the ellipse.

Every state calculated using a ray DNS shows no error except the climb rate. This behavior can be explained due to the fact that the climb rate from the flight data is the derivative of the barometric elevation measurements which has a slight delay compared to the actual

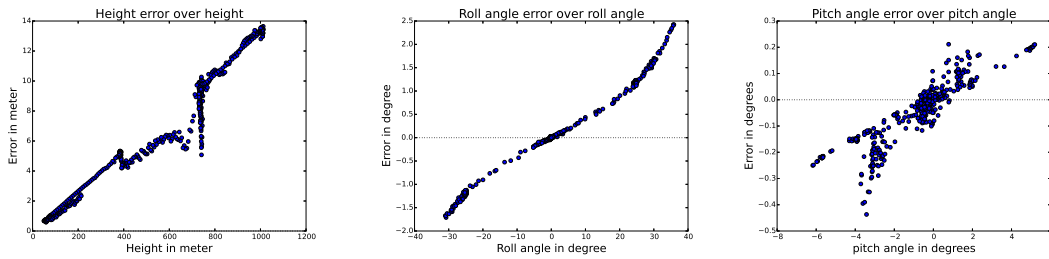


**Figure 6-4:** The error of the height, roll angle and pitch angle is proportional to the magnitude of the state. Each error is plotted against the state itself to demonstrate the effect.

**Table 6-1:** The root mean square error, the minimum error and the maximum error of the obtained states for an aircraft flying over flat terrain. FD 2 was used for a simulation with configuration J4,  $\beta_r = 45^\circ$  and  $\alpha_r = 40^\circ$ .

State [unit]	J4, $\alpha_r = 40^\circ$ and $\beta_r = 40^\circ$		
	RMS	min	max
Height [m]	7.86	0.59	13.65
Climb rate [m/s]	0.85	-3.25	2.84
Ground speed [m/s]	0.47	0.29	0.65
Phi [ $^\circ$ ]	0.89	-1.71	2.42
Theta [ $^\circ$ ]	0.12	-0.44	0.21
Alpha [ $^\circ$ ]	0.04	-0.10	0.11
Beta [ $^\circ$ ]	0.03	-0.09	0.10

vertical velocity.

The error of the ground speed,  $\alpha$  and  $\beta$  is less than  $0.5m/s$  for the ground speed and less than  $0.1^\circ$  for  $\alpha$  and  $\beta$ .  $\alpha$  and  $\beta$  are functions of the velocity measurement which means the accuracy of these states is not significantly affected by the change in shape of the ground projection.

## 6-5 Effect of Radar Depression Angle

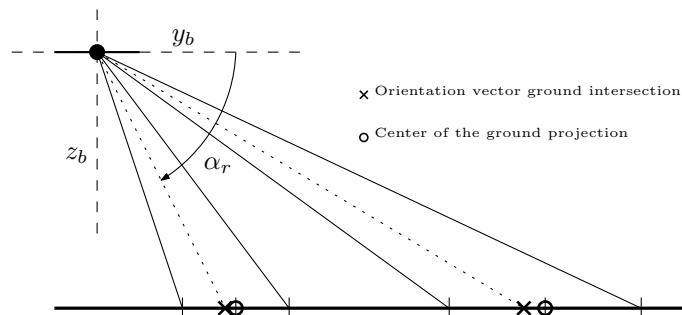


**Figure 6-5:** This figure shows the effect  $\alpha_r$  on the ground projection. As  $\alpha_r$  decreases the ground projection becomes an asymmetric ellipse and the center of that ellipse is not the center of the beam. Thus the averaging of the resulting VR spectrum does not represent the value of the VR pair of the ground in the center of the beam.

The depression angle  $\alpha_r$  ranges from  $0^\circ$  to  $90^\circ$ , where  $\alpha_r = 90^\circ$  is the radar oriented towards nadir and  $\alpha_r = 0^\circ$  is an orientation parallel to the Earth's surface. For a low  $\alpha_r$  the beam can lose sight of the ground in a steep roll where  $\phi > \alpha_r$ . Therefore the minimum value for  $\alpha_r$  are defined as  $\alpha_r < 40^\circ$ . However in some flights  $\alpha_r$  cannot be smaller than  $40^\circ$  due to aircraft maneuvers.

In straight horizontal flight, the projection of the beam on the ground is a perfect circle if  $\alpha_r = 90^\circ$ . However, when  $\alpha_r$  decreases, the projection becomes a slanted asymmetric ellipse with two different semi-major axes dependent on  $\alpha_r$  and the aircraft height AGL. As was shown in section 6-4 averaging the VR spectra generates an error if the ground projection of the beam is not symmetric. Therefore, a low  $\alpha_r$  should result in a larger error in the states than a high  $\alpha_r$ .

### 6-5-1 Flat Earth

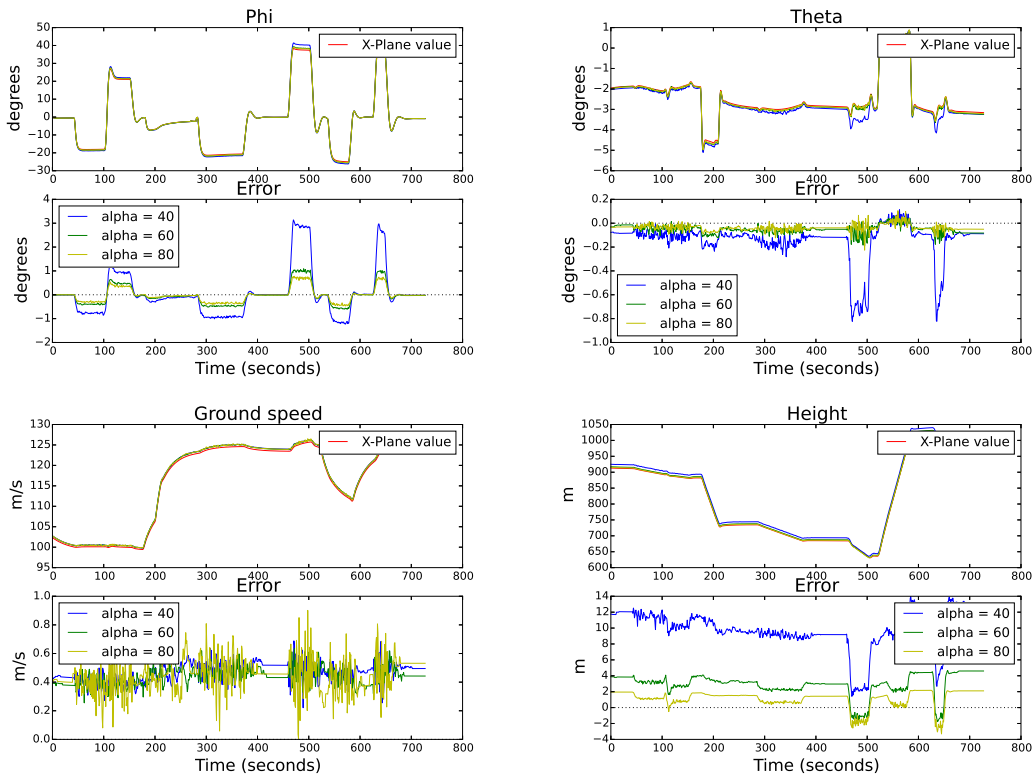


**Figure 6-6:** This figure shows the obtained height, phi, theta and ground speed and their errors for three simulations with FD 1, for different configurations. Each configuration is a J4 configuration with  $\beta_r = 45^\circ$ .  $\alpha_r$  is varied over the values  $40^\circ$ ,  $60^\circ$ ,  $80^\circ$ .

The effect of  $\alpha_r$  is first tested over a flat earth, eliminating other effects that could affect the states. The aircraft horizontal flight path is given in Figure A-1, however the DEM is set to zero. The radar configuration is J4 with  $\alpha_r = 40^\circ$ ,  $\alpha_r = 60^\circ$ , and  $\alpha_r = 80^\circ$ . The obtained states and the errors between the obtained states and the flight data are plotted in Figure B-2. The RMS error of each state is given in table 6-2 with the minimum and maximum error.

**Table 6-2:** The effect of  $\alpha_r$  on the root mean square error, the minimum error and the maximum error of the obtained states for an aircraft flying over flat terrain. FD 1 was used with a flat Earth DEM for the three simulation with configuration J4,  $\beta_r = 45^\circ$  and varying  $\alpha_r$ .

State [unit]	$\alpha_r = 40^\circ$			$\alpha_r = 60^\circ$			$\alpha_r = 80^\circ$		
	RMS	min	max	RMS	min	max	RMS	min	max
Height [m]	10.30	1.41	13.95	3.22	-1.77	4.67	1.52	-3.32	2.19
Climb rate [m/s]	0.95	-2.98	1.28	0.65	-2.84	1.29	0.61	-2.80	1.28
Ground speed [m/s]	0.47	0.22	0.69	0.45	0.26	0.63	0.46	0.00	0.90
$\phi$ [°]	0.95	-1.23	3.14	0.39	-0.61	1.09	0.28	-0.47	0.78
$\theta$ [°]	0.22	-0.82	0.11	0.06	-0.19	0.06	0.05	-0.23	0.10
$\alpha$ [°]	0.03	-0.12	0.12	0.01	-0.04	0.06	0.01	-0.04	0.04
$\beta$ [°]	0.03	-0.11	0.09	0.03	-0.11	0.11	0.07	-0.24	0.20

From Figure B-2 one can observe that the error of the height is smaller for large  $\alpha_r$ . This is reflected in the RMS error of the height. It is only at 1.52m for  $\alpha_r = 80^\circ$  but it can be as much as 10.30 for  $\alpha_r = 40^\circ$ .

The error of  $\phi$  shows a different behavior. The error is very close to zero every  $\alpha_r$  while  $\phi \approx 0^\circ$ . When in a roll, the error of  $\phi$  is proportional to  $\phi$  and inversely proportional to  $\alpha_r$ .

The same holds for  $\theta$  except that the error of  $\theta$  is also correlated to the error of  $\phi$  because of how it is determined in equation 3-31.

The climb rate shows similar behavior, with an overall larger error for low  $\alpha_r$ . However, four distinct peaks can be seen that correlate with an abrupt change in  $\theta$ .

The ground speed shows the error oscillating around 0.45m/s for all three values of  $\alpha_r$ . The error is slightly more unstable for  $\alpha_r = 80^\circ$  compared to the low  $\alpha_r$  with a maximum error of 1m/s.

$\alpha$  and  $\beta$  are determined very accurately as the error never exceeds  $0.11^\circ$  for  $\alpha$ , and  $0.24^\circ$  for  $\beta$ .

It can be concluded that there is a trend in the error of the height,  $\phi$ ,  $\theta$  and the climb rate. The error of these states is inverse proportional to  $\alpha_r$ . The ground speed,  $\alpha$  and  $\beta$  do not show significant correlation with  $\alpha_r$  because the error is very small for all  $\alpha_r$  settings.

### 6-5-2 Non-flat Earth

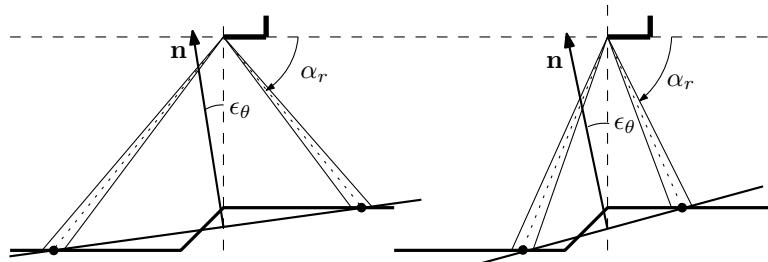


**Figure 6-7:** The effect of terrain for two configurations with a different  $\alpha_r$ . On the left:  $\alpha_r = 51^\circ$  and  $\epsilon_\theta \approx 8^\circ$ . On the right:  $\alpha_r = 68^\circ$  and  $\epsilon_\theta \approx 15^\circ$ .

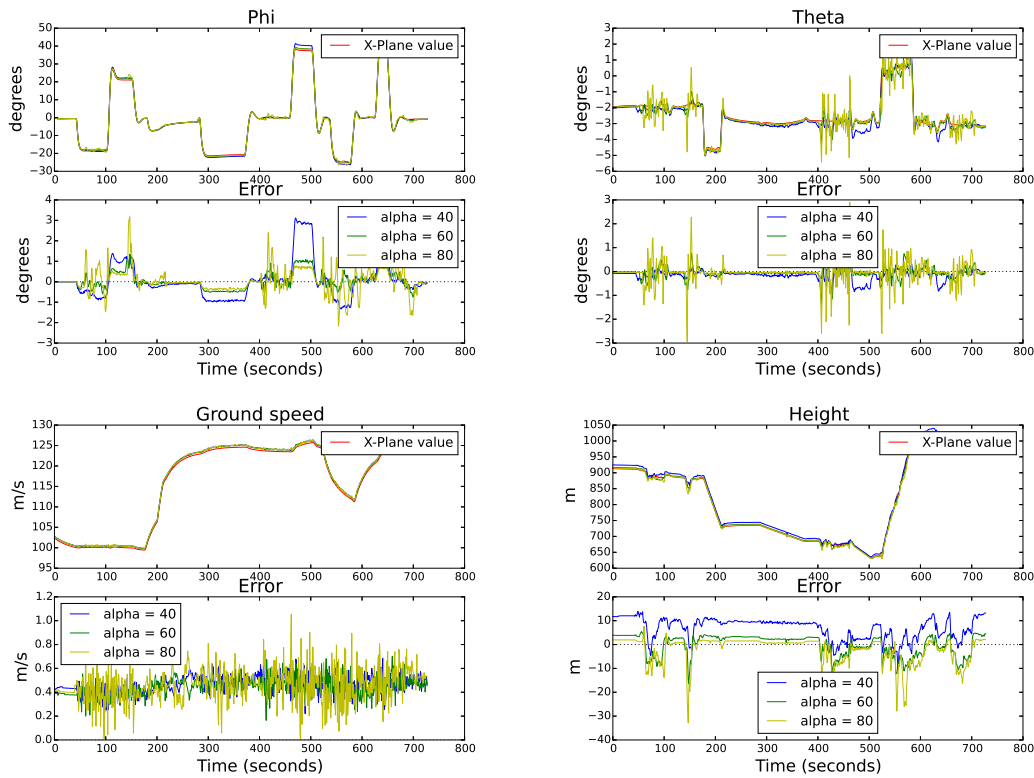


**Figure 6-8:** This figure shows the obtained height, phi, theta and ground speed and their errors for three simulations with FD 1, with varying  $\alpha_r$ . Each configuration is a J4 configuration with  $\beta_r = 45^\circ$ .  $\alpha_r$  has the values  $40^\circ$ ,  $60^\circ$  and  $80^\circ$ .

The same flight data was used as in subsection 6-5-1, the only difference is that a real DEM of the Netherlands was used to determine the height of the ground. The radar configuration is J4 with  $\alpha_r = 40^\circ$ ,  $\alpha_r = 60^\circ$ , and  $\alpha_r = 80^\circ$ . The obtained height, ground speed,  $\phi$  and  $\theta$  and their errors are plotted in Figure 6-8 as these are the relevant states. The other stats are shown in Appendix B. The RMS error of each state is given in table 6-3 with the minimum and maximum error.

The RMS error of every states is significantly larger than when flying over flat terrain no matter what the antenna configuration. It can be observed that the error caused by the terrain is added to the error caused by the beam width.

The states affected by the terrain are the height,  $\phi$  and  $\theta$ . This is because these states are calculated using the range measurement. The climb rate error has a large correlation with the error of  $\theta$  and  $\phi$ . Due to terrain variations, the plane calculated with the three range measurements can appear not to be horizontal while the aircraft is horizontal. This ambiguity has been shown in section 4-3.

The states  $\alpha$ ,  $\beta$  and ground speed are dependent on the velocity measurements and are not significantly affected by the difference in terrain.

Looking at Figure B-3 the effect of terrain is larger for a high  $\alpha_r$ . The error due to terrain is significantly larger for  $\alpha_r = 80^\circ$  compared to  $\alpha_r = 40^\circ$ . This can be explained by looking at the way the plane of the normal vector is created.

**Table 6-3:** The effect of  $\alpha_r$  on the root mean square error, the minimum error and the maximum error of the obtained states for an aircraft flying over non-flat terrain. FD 1 was used with a normal DEM for the three simulation with configuration J4,  $\beta_r = 45^\circ$  and varying  $\alpha_r$ .

State [unit]	$\alpha_r = 40^\circ$			$\alpha_r = 60^\circ$			$\alpha_r = 80^\circ$		
	RMS	min	max	RMS	min	max	RMS	min	max
Height [m]	8.22	-10.32	13.94	4.34	-16.32	5.43	5.88	-32.86	7.73
Climb rate [m/s]	0.95	-2.98	1.24	0.78	-3.12	2.30	1.12	-5.67	6.05
Ground speed [m/s]	0.47	0.22	0.69	0.45	0.16	0.70	0.48	0.00	1.06
$\phi$ [°]	0.96	-1.34	3.11	0.41	-0.76	1.36	0.59	-2.17	3.17
$\theta$ [°]	0.25	-0.84	0.32	0.24	-1.43	1.06	0.49	-2.95	2.90
$\alpha$ [°]	0.03	-0.12	0.11	0.02	-0.04	0.07	0.01	-0.04	0.04
$\beta$ [°]	0.03	-0.12	0.09	0.03	-0.11	0.11	0.08	-0.34	0.23

Figure 6-7 illustrates this with a 2D example of an aircraft flying horizontally. Two situations are represented: on the left, is the side view of an aircraft with two radars with a low  $\alpha_r$ , on the right the radars are oriented more towards the ground with a larger  $\alpha_r$ . In both situations the aircraft is perfectly horizontal, but the DNS measures an angle  $\theta$ . Even though the terrain is the same in both situations, the error measured in  $\theta$  is larger for the situation with a large  $\alpha_r$ .

The error due to terrain is the predominant one. The error is correlated to the terrain which, if unknown, is completely random. The error is also much larger in magnitude than the error caused by  $\alpha_r$  and the beam width. It can therefore be concluded that the states are more accurately determined with  $\alpha_r = 40^\circ$  when flying over non-flat terrain.

Finding a way to adapt the method of state determination to non-flat terrain could result in a great improvement of the aircraft states. This would also result in  $\alpha_r = 80^\circ$  as the best  $\alpha_r$  for this configuration.

## 6-6 Effect of Antenna Azimuth Angle

**Table 6-4:** The effect of  $\beta_r$  on the root mean square error, the minimum error and the maximum error of the obtained states for an aircraft flying over non-flat terrain. FD 1 was used with a flat Earth DEM for the three simulation with configuration J4,  $\alpha_r = 50^\circ$  and varying  $\beta_r$ .

State [unit]	$\beta_r = 20^\circ$			$\beta_r = 60^\circ$			$\beta_r = 80^\circ$		
	RMS	min	max	RMS	min	max	RMS	min	max
Height [m]	4.83	-13.65	8.50	4.92	-15.41	7.76	4.83	-14.07	7.57
Ground speed [m/s]	0.46	0.26	0.64	0.49	0.05	0.85	0.53	-0.60	1.62
$\phi$ [°]	0.51	-0.99	1.53	0.58	-0.70	1.80	0.65	-0.95	2.05
$\theta$ [°]	0.17	-0.88	0.46	0.24	-1.25	1.01	0.42	-1.85	2.04

The angle  $\beta_r$  has a small effect on the state accuracies compared to  $\alpha_r$ . The main difference is a slightly less accurate determination of the ground speed. For  $\beta_r = 80^\circ$  the error of the ground speed is much larger than the error when  $\beta_r$  is lower. The result for all the states is shown in Figure B-6. The height,  $\phi$ ,  $\theta$  and ground speed RMS error, and the minimum and maximum error are shown in table 6-4.  $\beta_r = 20^\circ$  and  $\beta_r = 60^\circ$  do not show much difference

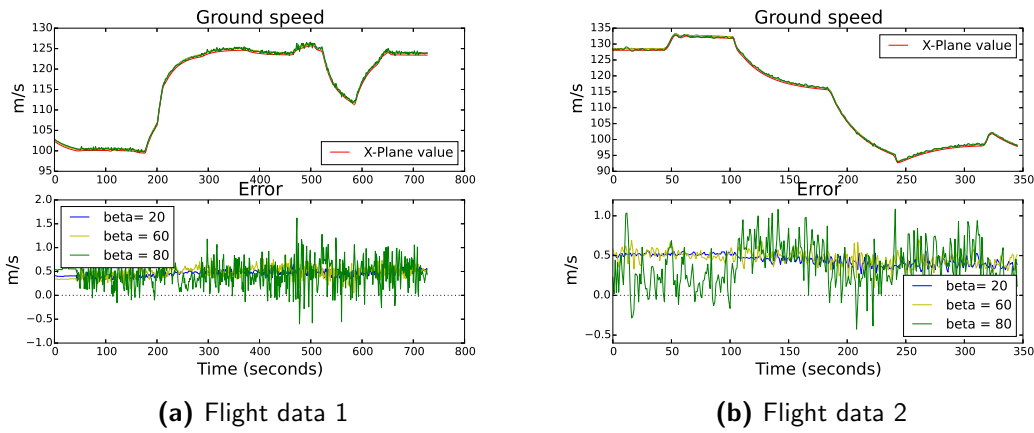


**Figure 6-9:** The obtained ground speed and the error for three J4 configurations with different  $\beta_r$  values. Two sets of three simulations are run, each set with a different flight data and each set with three different  $\beta_r$  values: 20°, 60° and 80°.

in accuracy, leading to the assumption that only large values for  $\beta_r$  impact the ground speed negatively.

The other states do not show any trend, this leads to the conclusion that the random terrain is the cause of the error. This terrain is different for each flight so cannot be taken into account on the basis of this result alone.

When  $\beta_r$  approaches 90° the minimum  $\alpha_r$  increases as the beam can rise above the horizon in a smaller turn. Therefore, to compare different values of  $\beta_r$ ,  $\alpha_r = 50^\circ$  has been chosen.

## 6-7 Effect of Terrain

Terrain causes an error in the height,  $\phi$  and  $\theta$  due to the assumption the earth is flat in the method used to calculate these states. The terrain effect result in the fact that radar configurations with  $\alpha_r = 40^\circ$  perform better than configurations with  $\alpha_r = 80^\circ$  that show less error over a flat earth.

The terrain error is larger in magnitude and it is random compared to the inherent error of the radar configuration. Therefore the error of the states over a flat Earth and non-flat Earth are plotted together in Figure 6-10. This illustrates the effect of the terrain on the obtained states combined with the effect of the beam width and  $\alpha_r$ . One can observe that the error of the terrain is added to the error due to the beam width and depression angle the system would have flying over flat terrain. Unlike the last two, the terrain error appears to be much larger in magnitude and random.

Therefore suppressing that error could improve the system significantly.

One way to adapt the model to terrain is to implement a terrain recognition module that can recognize the terrain using the height measurements. This could allow the position and attitude of the aircraft to be calculated using triangulation. Furthermore, this would permit the determination of  $\psi$  and make the DNS independent of a flux gate magnetometer.

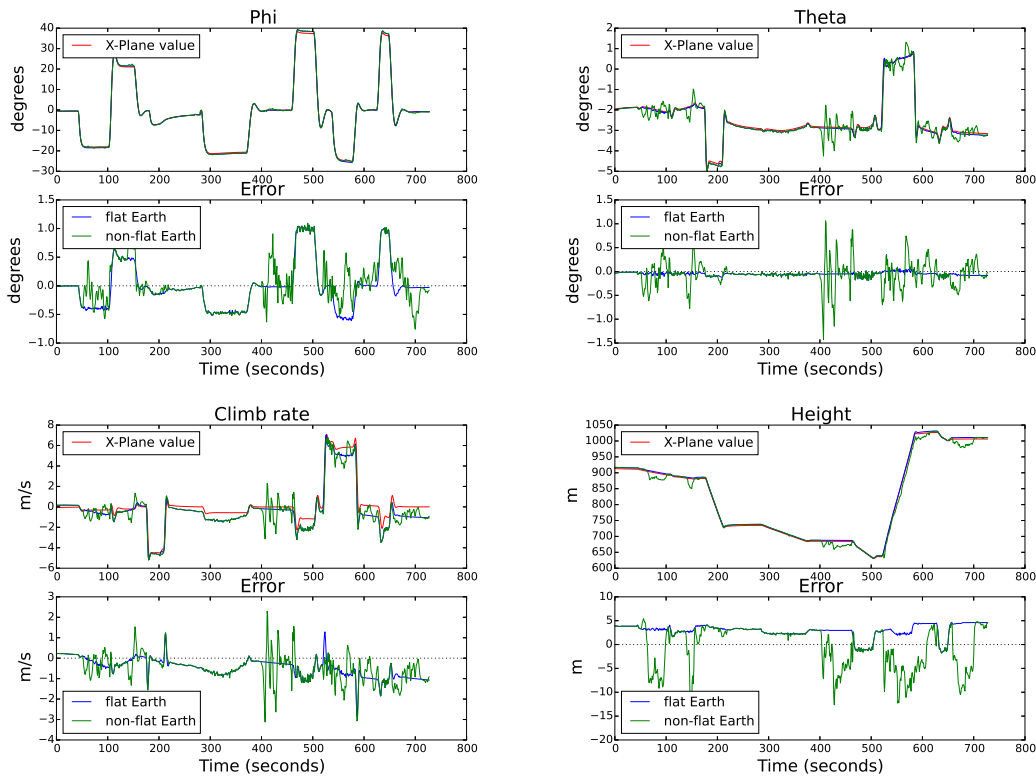


**Figure 6-10:** This figure shows the obtained height, phi, theta and ground speed and their errors for two simulations with FD 1, for different terrain. Each configuration is a J4 configuration with  $\beta_r = 45^\circ$  and  $\alpha_r = 60^\circ$ . The terrain is flat for one simulation, and for the other the DEM of Holland is used.

A second way would be to calculate the terrain height at the beams ground projections assuming the aircraft is in horizontal flight. Knowing this, the reference plane created with the measurement will not be compared to a flat plane, but to the plane that would be created if the aircraft would fly horizontally.

## 6-8 Navigation and Attitude Determination Performance

The navigation performance is measured by comparing the actual position of the aircraft with the position estimated using the states obtained with the DNS. The ground speed of the aircraft is used for dead-reckoning navigation. The horizontal position is determined by integrating the ground speed over time to calculate the distance traveled with the corresponding heading. Dead-reckoning navigation requires an initial horizontal position which is the first position from the flight data.

The vertical position is determined via direct measurement of the height with the DNS. The height can be transformed to elevation if the height of the terrain above MSL is known.

The attitude of the aircraft is also determined with direct measurements of the DNS. The accuracies of  $\phi$  and  $\theta$  have been described in the sections above. Only  $\psi$  is an unknown which

has to be measured using a different sensor.

### 6-8-1 Horizontal navigation performance

The ground track of the aircraft is calculated in  $F_E$  with:

$$\Delta x = v_{gs} \cos \psi t \quad (6-2)$$

and

$$\Delta y = v_{gs} \sin \psi t \quad (6-3)$$

The x- and y- coordinates can be transformed to latitude and longitude coordinates with:

$$\Phi = \frac{\Delta x}{R_{Earth}} \frac{180}{\pi} \quad (6-4)$$

and

$$\lambda = \frac{\Delta y}{R_{Earth} \cos \Phi} \frac{180}{\pi} \quad (6-5)$$

with:  $R_{Earth} = 6371000m$

and  $t = 1s$

$v_{gs}$  is the only state that affects the accuracy of horizontal navigation and the accuracy of  $v_{gs}$  does not significantly change with different radar configurations. The results of the horizontal navigation performance is given in Figure 6-11 where three flights have been simulated. For each case the DNS configuration is J4 with  $\alpha_r = 40^\circ$  and  $\beta_r = 45^\circ$ .

Table 6-5 summarizes the vertical and horizontal navigation error for each data set. The horizontal error increases every second with the ground speed error. The absolute maximum error is 455m after 278 minutes of flight for FD 1 with this DNS configuration and the maximum error is 111m after 344 minutes for FD 3. The horizontal error of the second flight does not show the same increasing trend over time that is a characteristic of dead reckoning navigation, which is probably due to the aircraft maneuvers. The maximum error of the second flight is 128m after 243 seconds. The accuracy of the ground speed does not change significantly with a different configuration, therefore, the magnitude of error depends mostly on the aircraft maneuvers.

**Table 6-5:** Navigation performance for each set of flight data.

Flight data	Vertical error [m]		Horizontal error [m]	Flight duration [s]	Distance traveled [m]
	max	RMS	max		
FD 1	13.9	8.22	455	728	84339
FD 2	13.6	7.86	128	475	56409
FD 3	18.5	9.47	111	344	39146

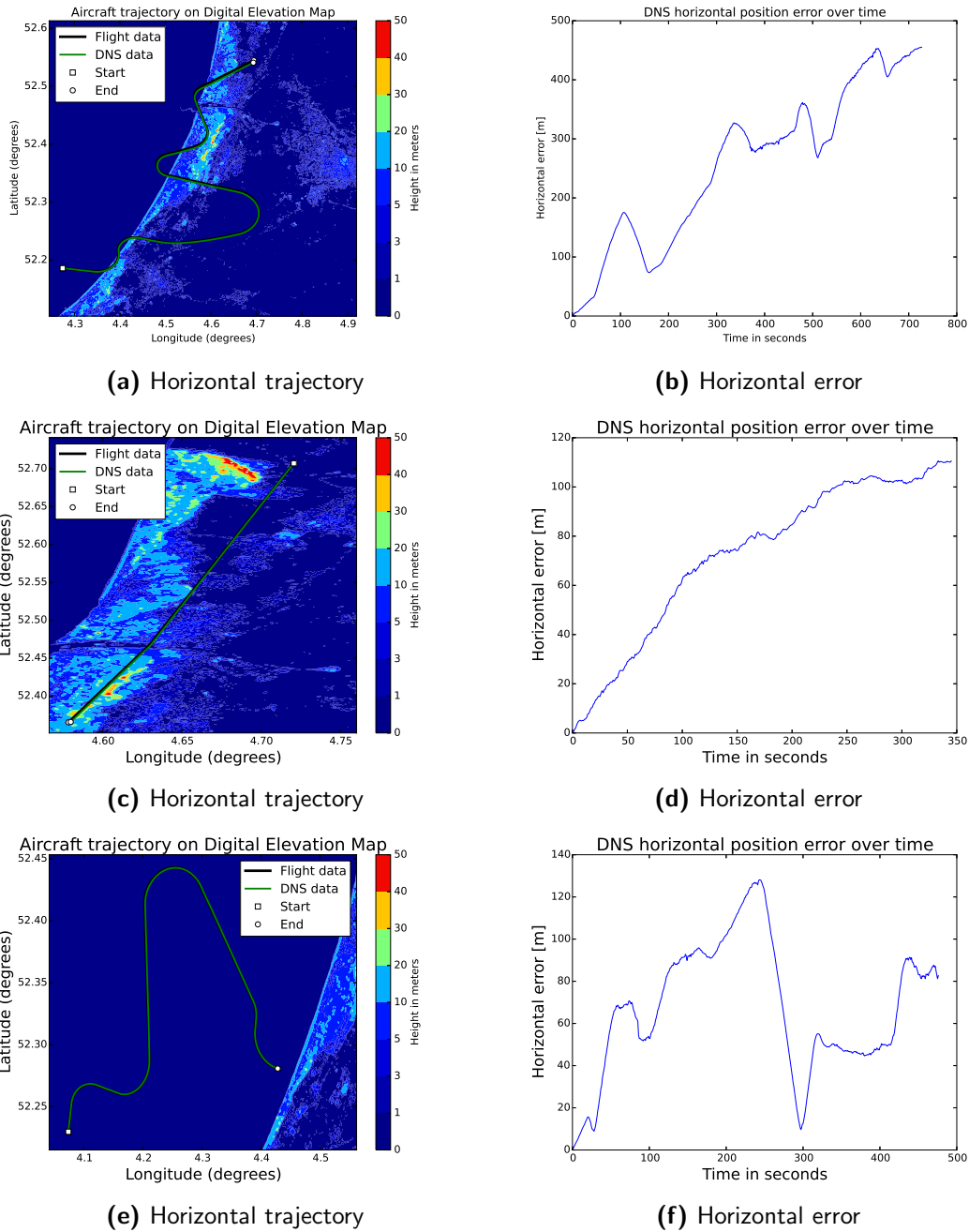
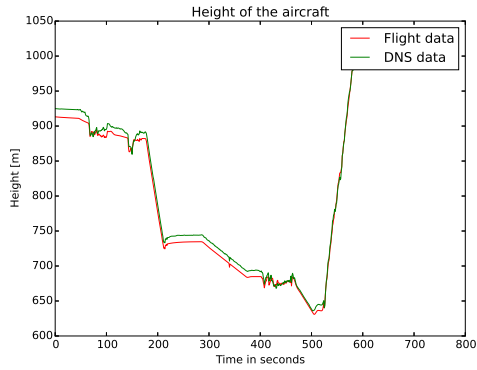
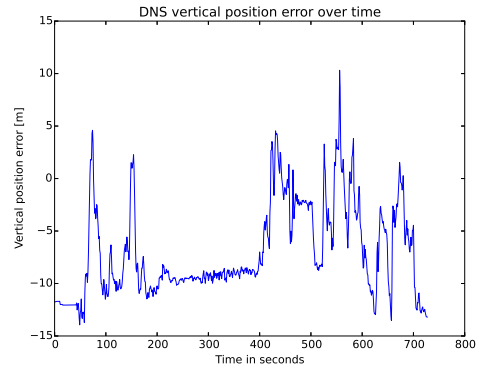


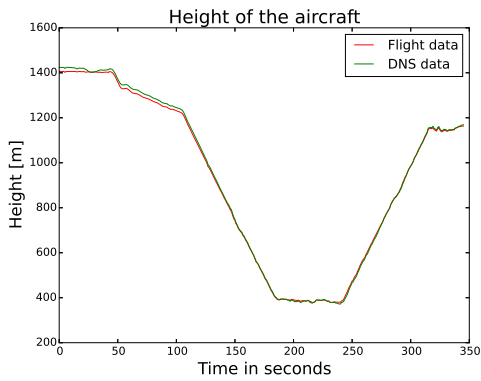
**Figure 6-11:** The figures on the left show the obtained horizontal trajectory against the flight data trajectory, for the different flight data. The figures on the right show the error of the horizontal position over time.



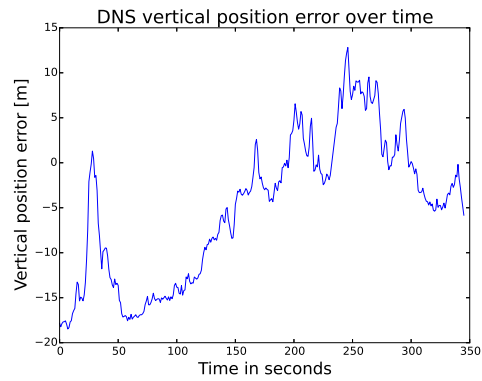
(a) Aircraft height



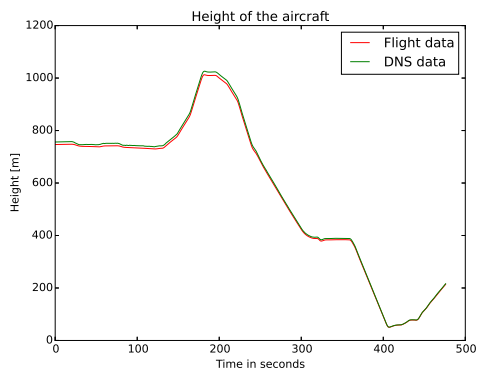
(b) Vertical error



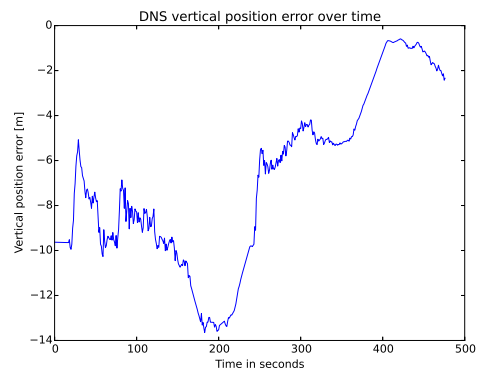
(c) Aircraft height



(d) Vertical error



(e) Aircraft height



(f) Vertical error

**Figure 6-12:** The figures on the left show the obtained height against the flight data height, for the different flight data. The figures on the right show the vertical position error over time.

### 6-8-2 Vertical navigation performance

The vertical position of the aircraft is determined by measuring the height of the aircraft. Therefore, it does not increase over time like the horizontal position error. The height and the height error of the three flight simulations are plotted in Figure 6-12 and the maximum error and the RMS error are listed in table 6-5. The same configuration was used as explained above. The absolute vertical error has a maximum of  $13.94m$  and the RMS error is  $8.22m$  for the first flight. For the second flight, the maximum error is  $13.6m$  and the RMS error is  $7.86m$ . For the third flight, the maximum error is  $18m$  and the RMS error is  $9.47m$ .

### 6-8-3 Attitude determination performance

**Table 6-6:** Attitude determination performance for each set of flight data.

Flight data	Roll angle error $^{\circ}$		Pitch angle error $^{\circ}$	
	max	RMS	max	RMS
FD 1	3.11	0.96	0.84	0.25
FD 2	2.42	0.89	0.44	0.12
FD 3	0.60	0.25	0.84	0.27

The attitude of the aircraft is composed of the angles  $\phi$ ,  $\theta$  and  $\psi$ . The angles  $\phi$  and  $\theta$  can be determined with the DNS, but  $\psi$  cannot be determined with the current DNS. The accuracies of the obtained states calculated with the flight data sets FD 1, FD 2, and FD 3, are shown in table 6-3. The DNS configuration is J4 with  $\alpha_r = 40^{\circ}$  and  $\beta_r = 45^{\circ}$ .

The errors of  $\phi$  and  $\theta$  are given in table 6-6. The maximum absolute errors for  $\phi$  are quite significant, but the roll angle error only exceeds  $1^{\circ}$  when the aircraft is in a roll of at least  $20^{\circ}$ . This was shown in Figure 6-4. The maximum error for  $\theta$  for FD 1 is  $0.84^{\circ}$  and the RMS is  $0.25^{\circ}$ . The  $\theta$  error for FD 2 is relatively smaller due to the flat terrain of FD 2.

## 6-9 Optimal Radar Configuration

**Table 6-7:** Error in the calculated states for varying number of on-board antennas.

State [unit]	4 antennas			5 antennas			6 antennas		
	RMS	min	max	RMS	min	max	RMS	min	max
Height [m]	4.78	-10.00	7.95	5.44	-19.23	9.28	4.92	-13.36	8.89
Ground speed [m/s]	0.47	0.27	0.77	0.46	0.22	0.74	0.47	0.24	0.66
$\phi$ $^{\circ}$	0.52	-0.68	1.50	0.61	-1.01	1.95	0.60	-0.75	1.86
$\theta$ $^{\circ}$	0.18	-1.06	0.48	0.18	-0.82	0.55	0.17	-0.79	0.44

As discussed above, the effect of alpha does appear to be a very important factor for the accuracy of the states. However, this depends on the terrain profile. A flat earth requires a very large  $\alpha_r$  to work optimally, but when the terrain is not flat, a smaller angle  $\alpha_r$  performs better.

Using more than 4 antennas does not show a significant change in state accuracies. This is shown in Table 6-7 where three configurations with the same  $\alpha_r$  are tested.

Terrain has a very large influence on the accuracy of the height,  $\phi$  and  $\theta$ . Multiple different configurations have been tested to find an optimum one. However, as the error is dependent on the terrain, a single configuration is not optimal for all the possible flight scenarios.

The following results for antenna configurations can be summarized:

- Configurations consisting of radars with high  $\alpha_r$ , such as  $\alpha_r = 80^\circ$ , perform best on flat Earth.
- Configurations consisting of radars with low  $\alpha_r$ , such as  $\alpha_r = 40^\circ$ , perform best on non-flat Earth.
- Configurations with  $\beta_r$  approaching  $90^\circ$  require higher a  $\alpha_r$  in order to keep track of the ground.
- Increasing the amount of antennas does not significantly affect the state accuracies.

---

## Chapter 7

---

# Conclusion

This thesis has presented an investigation into whether multiple Collision Avoidance Radars developed by Selfly ED&A can be used in a Doppler Navigation System to support the pilot in navigation and attitude determination in Visual Flight Rules flight. A Python model has been created for this purpose and it has been used to determine which factors affect the accuracy of the aircraft states measured with the Doppler Navigation System. This knowledge is used to optimize the radar configuration to give the best estimates of the aircraft states.

In VFR flight the pilot has to perform the following tasks visually: See and Avoid, navigation, and attitude determination. Selfly ED&A has developed a Collision Avoidance Radar which can help the pilot Detect and Avoid. This radar is cheap, light, small and can be mounted on almost every part of a general aviation aircraft. This thesis has therefore been set up to determine if the Collision Avoidance Radar could also support the pilot for navigation and attitude determination.

The goal of this thesis was to assess the performance of a Doppler Navigation System consisting of Frequency Modulated Continuous Wave radars developed by Selfly ED&A. The performance is measured directly comparing the obtained aircraft states with the flight data, and indirectly by using the obtained states for dead-reckoning navigation and comparing the horizontal and vertical position of the aircraft with position from the flight data.

The on-board radars are oriented towards the ground and measure both velocity and range of the ground clutter. The velocity measurements are used to determine the 3D velocity vector of the aircraft in  $F_b$  and the range measurements can be used to geometrically determine the attitude and the height of the aircraft. From this, the following aircraft states required for navigation and attitude determination can be computed: height, ground speed, roll angle and pitch angle.

The heading is a state that cannot be obtained with just the radar velocity and range measurements and has to be obtained with another sensor such as a magnetometer. With the heading angle, the DNS can be used for dead-reckoning horizontal navigation by integrating the velocity over time.

The orientation of each radar on the aircraft is described with the depression angle  $\alpha_r$  and the azimuth angle  $\beta_r$ .  $\alpha_r$  is the angle between the horizontal plane of the aircraft and its vertical axis.  $\beta_r$  is determined the same way as the heading angle but with the aircraft longitudinal axis as  $0^\circ$ .

A model was created in Python which models the Doppler Navigation System using flight data and radar parameters. The radar signal modeling could not be integrated because of the long computation time of the signal generation module. Therefore, the velocity range data calculated geometrically is used instead for the state determination. The model can also be used in a real flight test where the signal generation module is not used.

The simulation results show that a configuration consisting of radars with  $\alpha_r = 80^\circ$  can determine the aircraft states more accurately than with a low  $\alpha_r = 40^\circ$  on flat terrain. This is a result of averaging the VR spectrum to a single VR pair due to the large beam width of this particular FMCW radar. On non-flat terrain the opposite is true because of the way the normal vector is defined, resulting in a smaller constant error for low  $\alpha_r$ , compared to a large  $\alpha_r$ .

The number of antennas does not significantly improve the accuracy of the states or the navigation performance, neither does combining large  $\alpha_r$  with low  $\alpha_r$  in the same configuration. The effect of  $\beta_r$  does not show any significant correlation with the accuracy of the states, except for the ground speed accuracy which is reduced when  $\beta_r$  approaches  $90^\circ$ .

The results from three simulations show that an aircraft horizontal position can be determined with an accuracy of at least  $455m$  for a  $728s$  flight in which the aircraft traveled  $84.332km$  and the vertical position with an accuracy of at least  $18m$ . The attitude of the aircraft is composed of the three Euler angles:  $\phi$ ,  $\theta$  and  $\psi$ . The angle  $\phi$  can be determined with a maximum error of  $3.11^\circ$  and a RMS error of  $0.96^\circ$  during a  $728s$  flight over terrain varying in height between  $0m$  and  $30m$ .  $\theta$  has a maximum error of  $0.84^\circ$  and a RMS of  $0.27^\circ$  over the same flight.

These results show that the horizontal navigation error is dependent on time but a  $455m$  error over 12 minutes is low enough to be used in case of emergency. This means that this system could be used in situations where the pilot has to fly through a cloud. The vertical navigation error is not dependent on time and stays within  $20m$  at all time during the simulations. This is well within the pilots safety margins and altimeter precision.

The error of the roll angle is proportional to the roll angle itself with a maximum error of  $3.11^\circ$  for  $40^\circ$ . In steady horizontal flight the roll angle error stays well within  $1^\circ$ . The pitch angle error stays within  $1^\circ$  as well. Therefore the attitude can also be determined accurately enough for a short flight with no visibility.

The terrain is the main source of error in the estimation of  $h$ ,  $\phi$ ,  $\theta$ , because it is unknown and a flat earth is assumed in the calculation. Reducing this error could significantly improve the performance of the system. This can be done using a Digital Elevation Map in the calculation of the states by estimating the ground plan orientation which is used as reference for the state determination. Another way to remove this error is to use terrain recognition to determine the exact geographical position where the beam hits the ground. This makes it possible to determine the aircraft attitude and position via triangulation.

The results of the simulations show that Collision Avoidance Radars developed by Selfly ED&A can be used in a Doppler Navigation System to navigate and determine the attitude

of an aircraft flying VFR with no visibility for a short period of time. The system could even be improved by coupling it to a Digital Elevation Map to reduce the error caused by terrain.



---

## Chapter 8

---

# Recommendations

The following chapter discusses points of improvement for the accuracy of the states, and recommendations to improve the model.

### 8-1 Improve the terrain error

The current DNS model cannot determine the heading of the aircraft. Furthermore, the terrain causes a large error in some aircraft states. Both these problems can be solved if the radars could recognize the terrain it measures and use a Digital Elevation Map to associate a geographic position to each measurement. Knowing the geographic position of three points on the Earth, the distance of each point to the aircraft and the orientation of the aircraft with respect to each point, is enough to determine the aircraft position and attitude via triangulation. This scenario permits the determination of the heading as well.

It is also possible to improve this model by reducing the terrain error, coupling it to a Digital Elevation map. The geographic position of the aircraft, the heading and the orientation of the antennas can be used to create a plane of the terrain for an aircraft flying horizontally. The error that is then measured in the states is much smaller because the terrain is not assumed flat.

The error caused by terrain in the states  $\phi$  and  $\theta$  has a very distinct characteristic. It causes a very fast, almost instantaneous change in the state. These rapid changes are not normal aircraft behavior as they normally increase or decrease gradually over a period of time. Therefore it would be possible to recognize this characteristic behavior and filter it out.

### 8-2 Flight data acquisition

The flight data acquisition module should be part of the main program by integrating it in the GUI. The flight data acquisition module is run separately from the simulation but it should

be integrated in the GUI allowing the user to create flight data from X-Plane with the same GUI that runs the simulations.

There should be more real time feedback during the acquisition of flight data. Especially with the constrain on geographical position with the DEM, the flight data acquisition module should warn the user in X-Plane when for example the aircraft flies outside the DEM area.

### 8-3 Signal processing

This thesis focused on the method to compute the aircraft states assuming VR data was perfect. Not taking into account noise and other parameters that affect the radar signal. This assumption was made as a result of the long computation times of the signal generation module in the model. It was therefore impossible to integrated that module in the simulations. The signal processing module could therefore not be integrated either because a signal could not be generated and no existing radar signal data was available.

In order to integrate the signal generation module, it should be made much faster.

In order to integrate the signal processing module, a radar signal should be available, this can be a real radar data or a generated signal using the signal generation module.

The state determination method assumes a single VR pair per radar. This pair is obtained by averaging all the VR pairs from the ground clutter and the assumption is made that this can also be done for the VR spectrum. The averaging does not take into account power differences in the signal due to the distance of the ground to the radar and the reflectivity of the ground. Therefore, this method of transforming the VR spectrum to a single VR pair should be validated.

There might be more information in the spectrum of the ground clutter than just a single VR pair, such as the phase difference of the ground between the receivers, this could also be taken into account when determining the states.

### 8-4 Graphical User Interface

The number of antennas is limited to 6 when creating a radar configuration. This should be increased for more complex configurations.

Currently only four standard configurations are hard coded in the GUI. It would be better allow the user to create his own configurations, and alter existing ones.

Create a preview of the flight data selected, showing the horizontal and vertical trajectory upon selection of the flight data.

Create a preview of the radar configuration by showing an image of the radars on an aircraft upon selecting the configuration.

This model uses only one DEM file type for the simulations. However, DEMs come in a variety of accuracies and formats. The effect of the DEM on the accuracy of the system should also be investigated. Therefore, there should be an option to change the DEM accuracy in the GUI.

## 8-5 Simulation improvements

Make the program robust for missing data due to for example: too high roll angles. Currently, the simulation is aborted when one of the radars does not see any terrain.

Make the simulation real time so it can be run while flying the flight simulator with display showing the calculated states. The main bottleneck now lies in the signal generation which is extremely computationally intensive.

The model could be used online during a real flight test, because the signal generation module is not necessary if the state determination module is connected directly to multiple radars. A flight test should be flown with a DNS radar configuration to validate the model with real flight data.

In this thesis, the water is assumed to be still, which is important when measuring the relative radial velocity of the water. When flying over water, or moving objects, the velocity will be added to the velocity of the aircraft in the velocity measurement. The effect this can have on the accuracy of the states should also be investigated.



---

# Appendix A

---

## **Flight data**

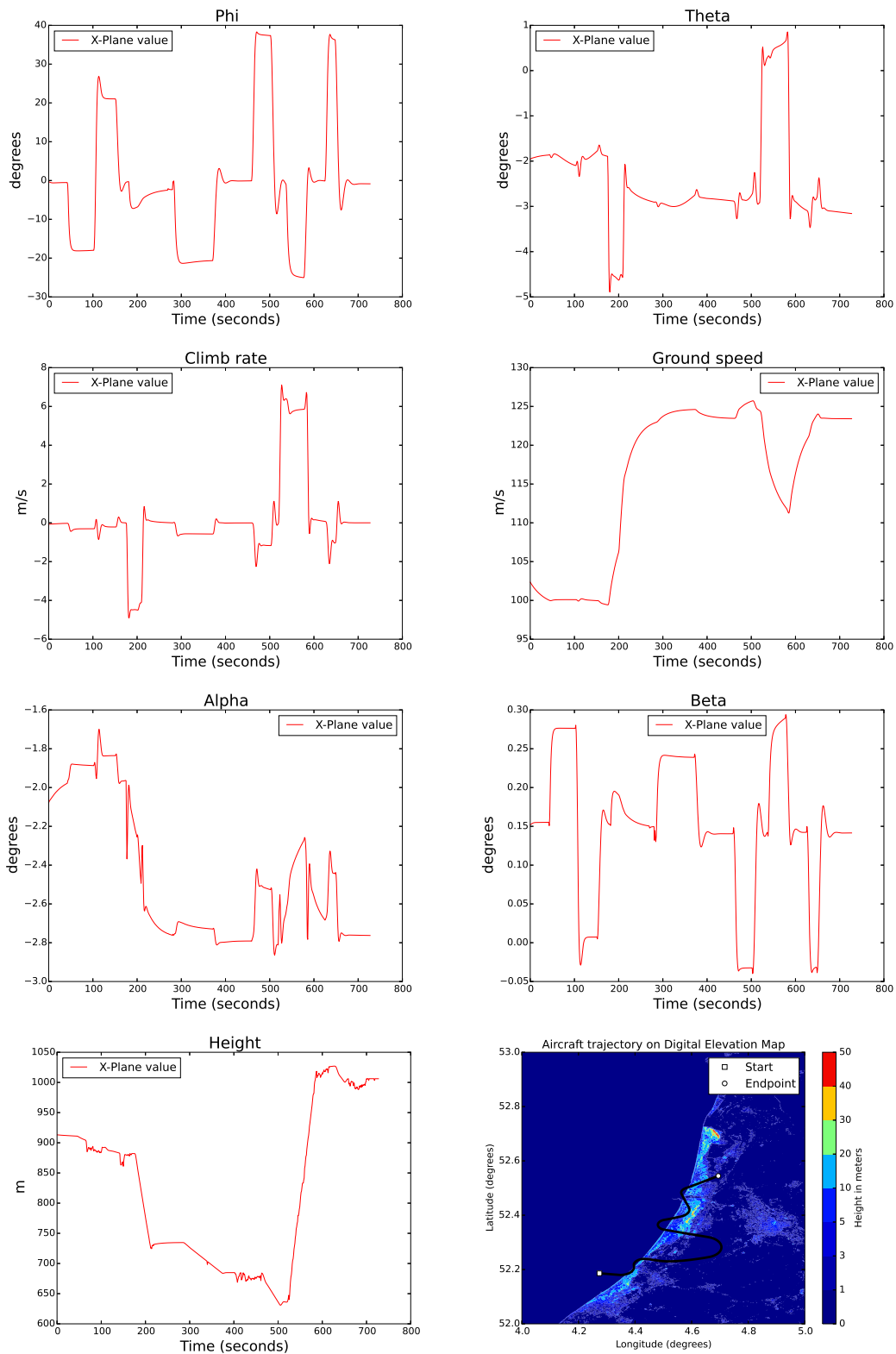


**Figure A-1:** The states from the flight data file Flight Data 1. This is flight data of a flight of 728 seconds over non-flat terrain.

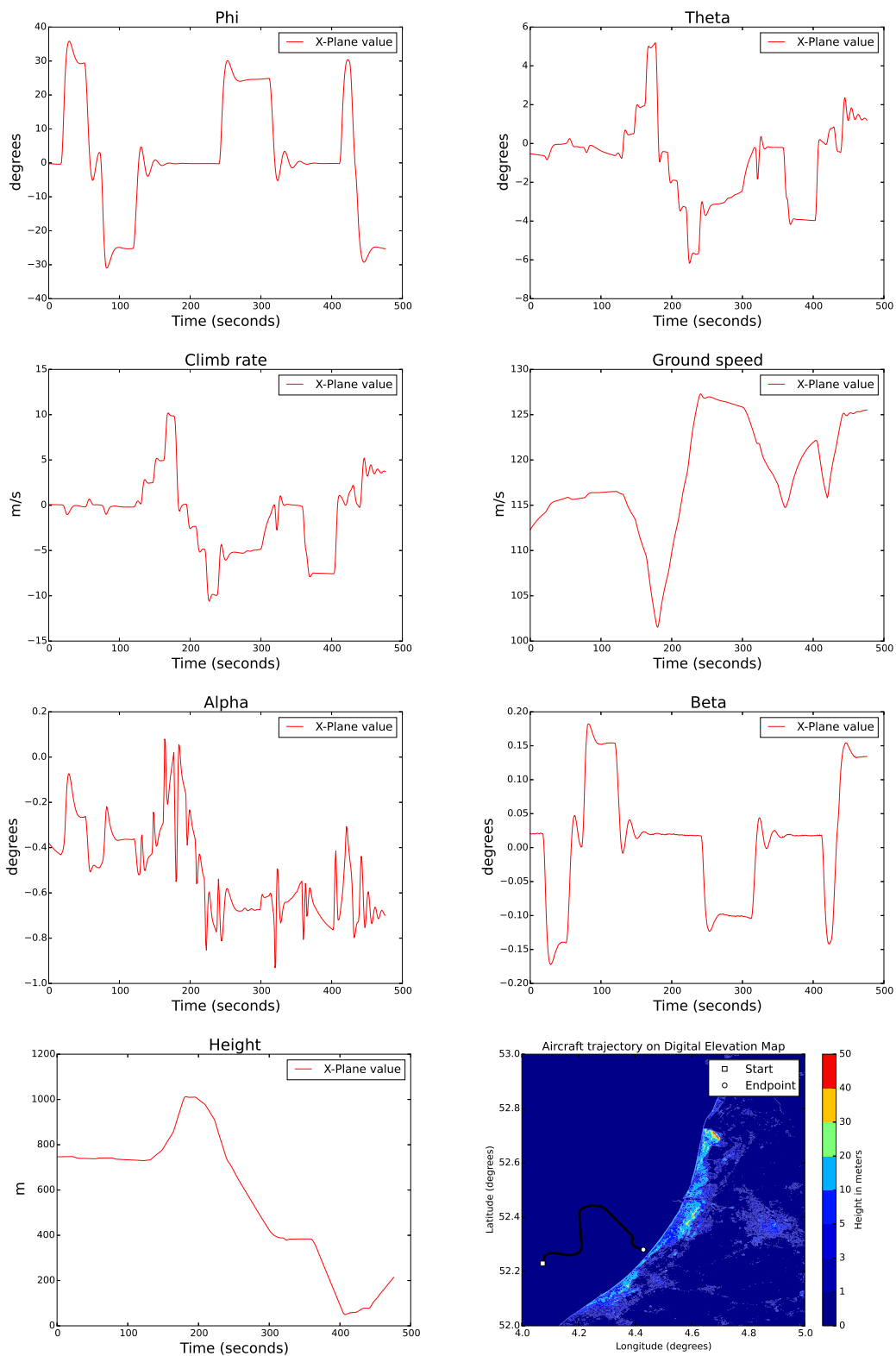


**Figure A-2:** The states from the flight data file Flight Data 2. This is flight data of a flight of 475 seconds over flat terrain.

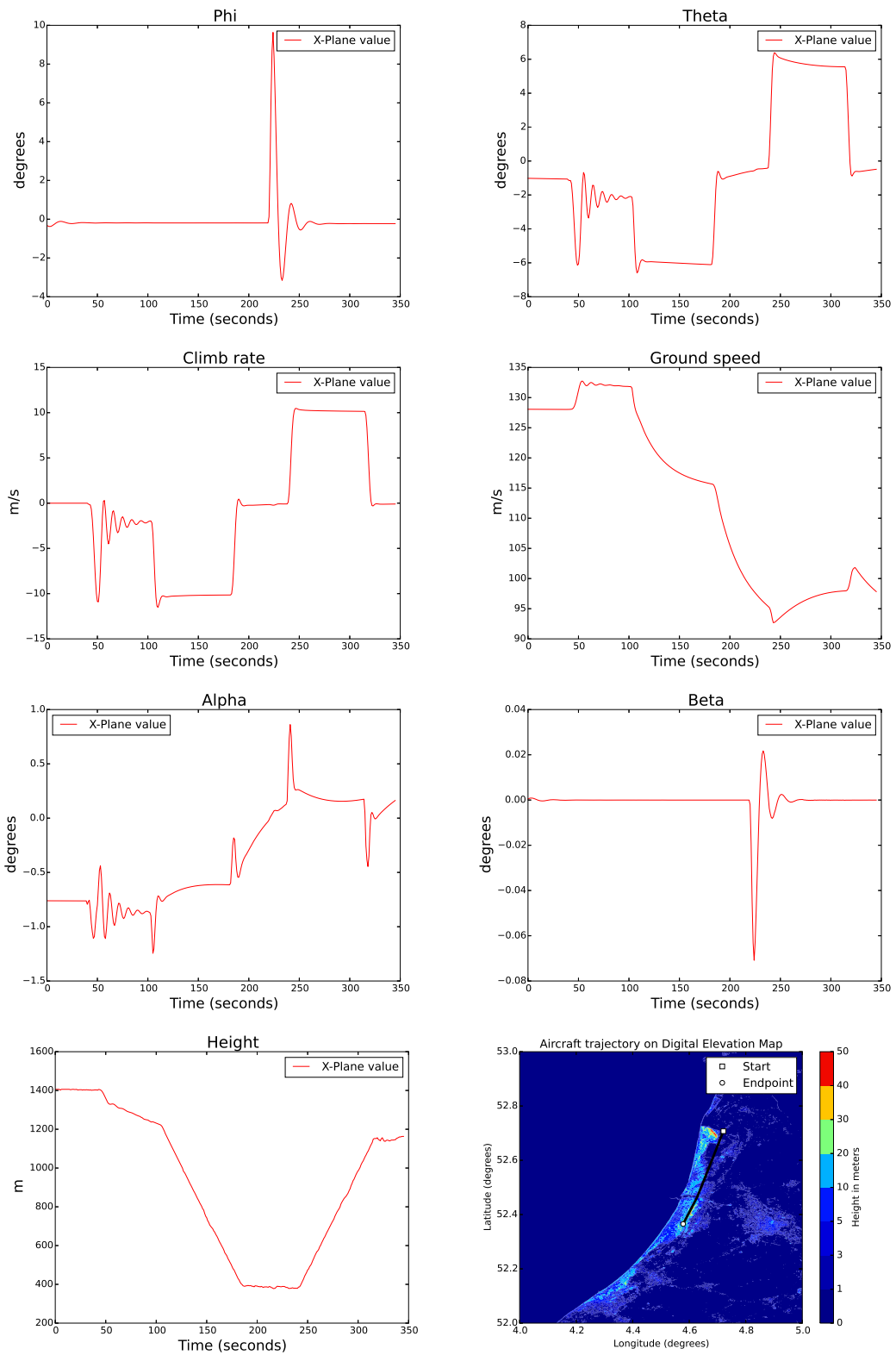


**Figure A-3:** he states from the flight data file Flight Data 3. This is flight data of a flight of 344 seconds over non-flat terrain.

---

## Appendix B

---

### Simulation results

This appendix contains the results of the simulations. Each set of results is obtained varying the Flight Data, the Digital Elevation Map and the radar configuration.

The results of the state determination are plotted using two subplots per state. The upper subplot contains the value of the state over time expressed in degree, meter, or meter per second, depending on the state. The red line in the upper subplot is the reference which is directly read from the flight data. The other lines are the states calculated using DNSs. Multiple lines means multiple DNS configurations are being represented.

The lower subplot shows the difference between the reference state and the calculated state. The error is calculated as follow:

$$\epsilon = x_{fd} - x_{obt} \quad (\text{B-1})$$

With,  $\epsilon$ : the error.

$x_{fd}$ : the reference state from the flight data.

$x_{obt}$ : the obtained state from the DNS

The vertical axis shows the error in the same unit as the subplot above. Each line in the upper subplot has an error line of the same color in the lower subplot.

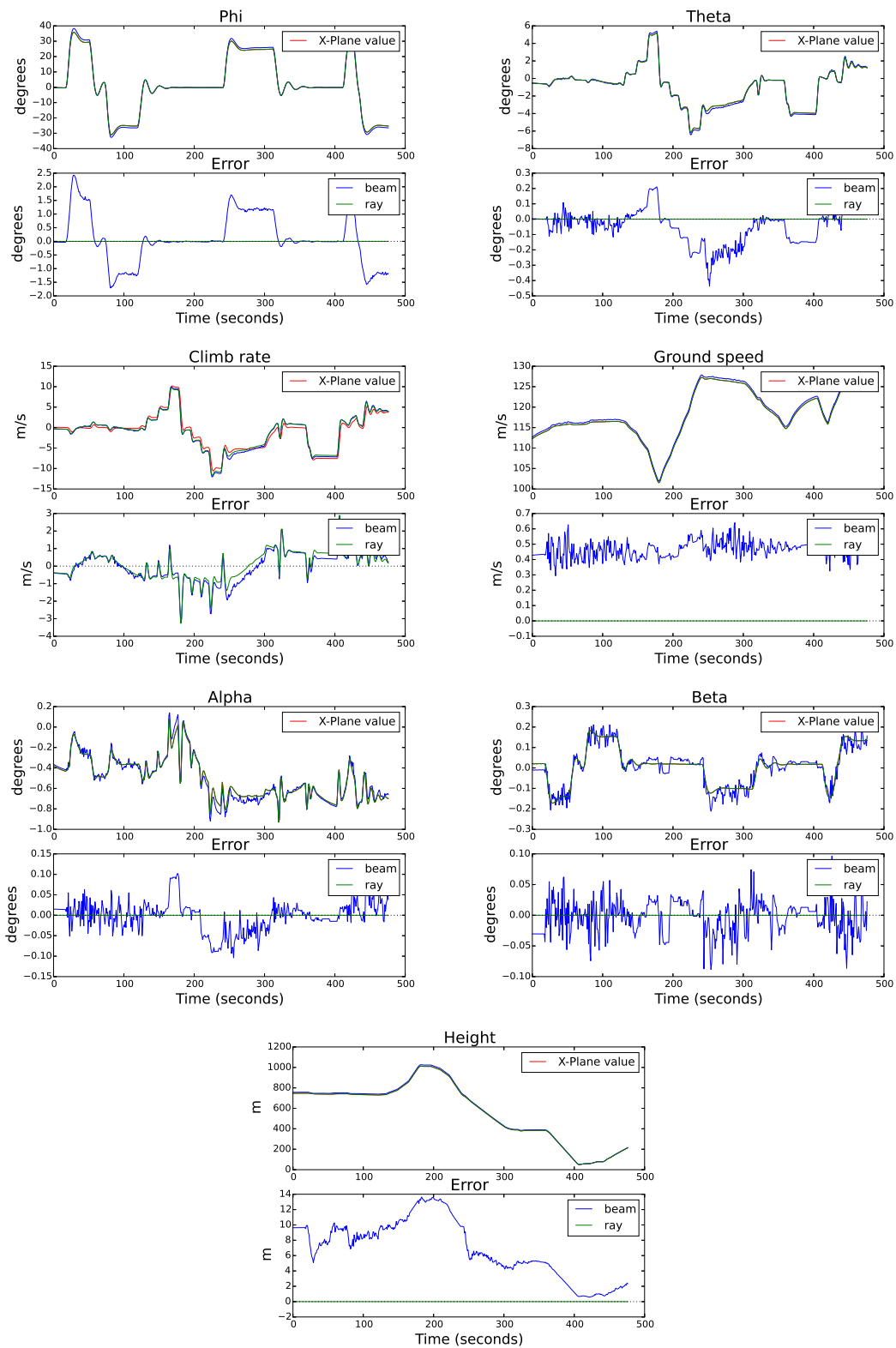


**Figure B-1:** The effect of the beam width on the state error with Flight Data 2. Two simulations have been performed with the same configuration but a different aperture angle. The aperture angle for the beam is  $10^\circ$  and for the ray  $> 1^\circ$ . The radar configuration is J4 with  $\alpha_r = 40^\circ$  and  $\beta_r = 45^\circ$ .

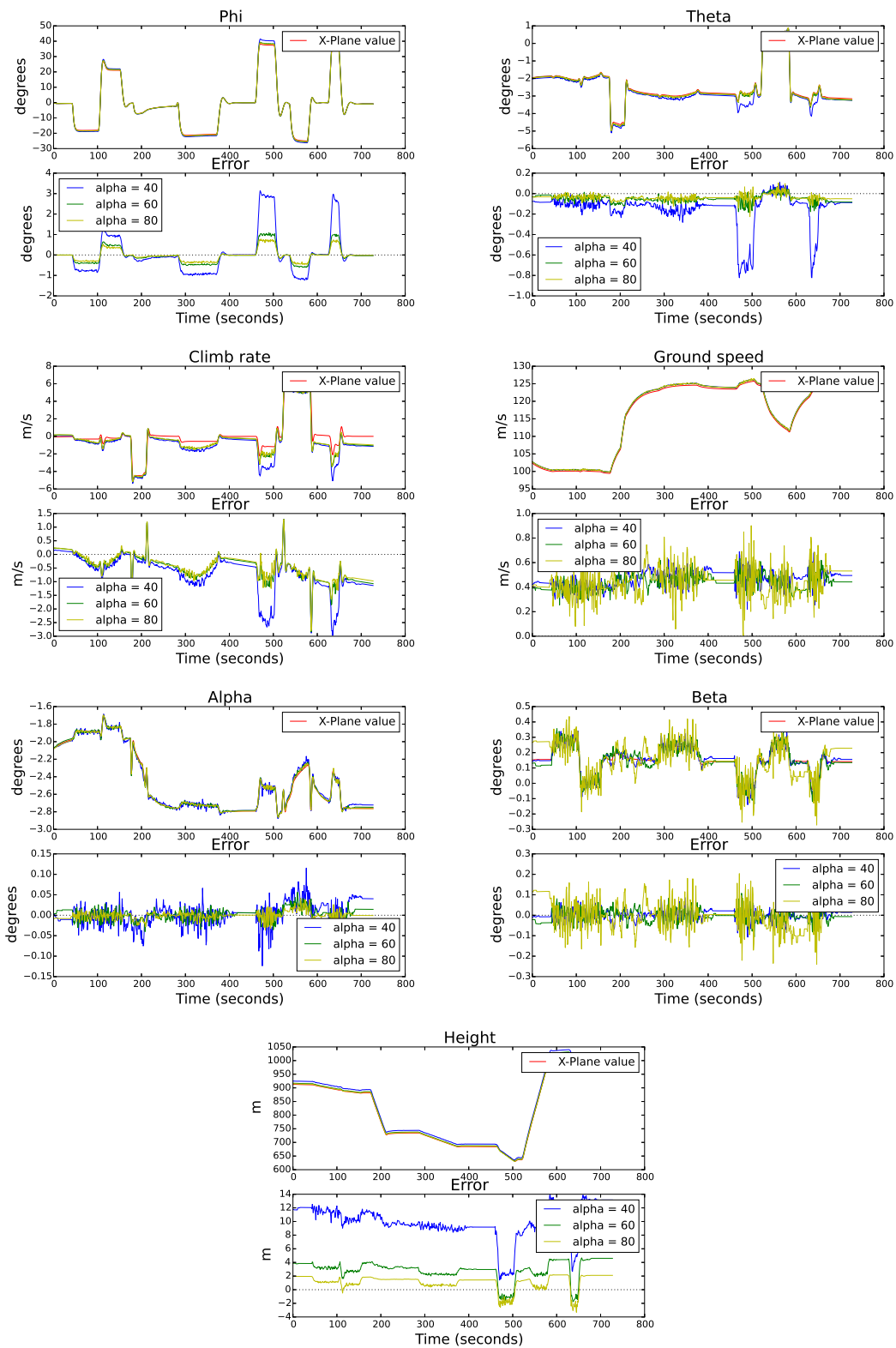


**Figure B-2:** The effect of  $\alpha_r$  on the states over a flat Earth. Three simulation are performed using Flight Data 2 where the configuration is J4 with  $\beta_r = 45^\circ$ . The value of  $\alpha_r$  is different for each simulation, and has values:  $40^\circ$ ,  $60^\circ$  and  $80^\circ$ .

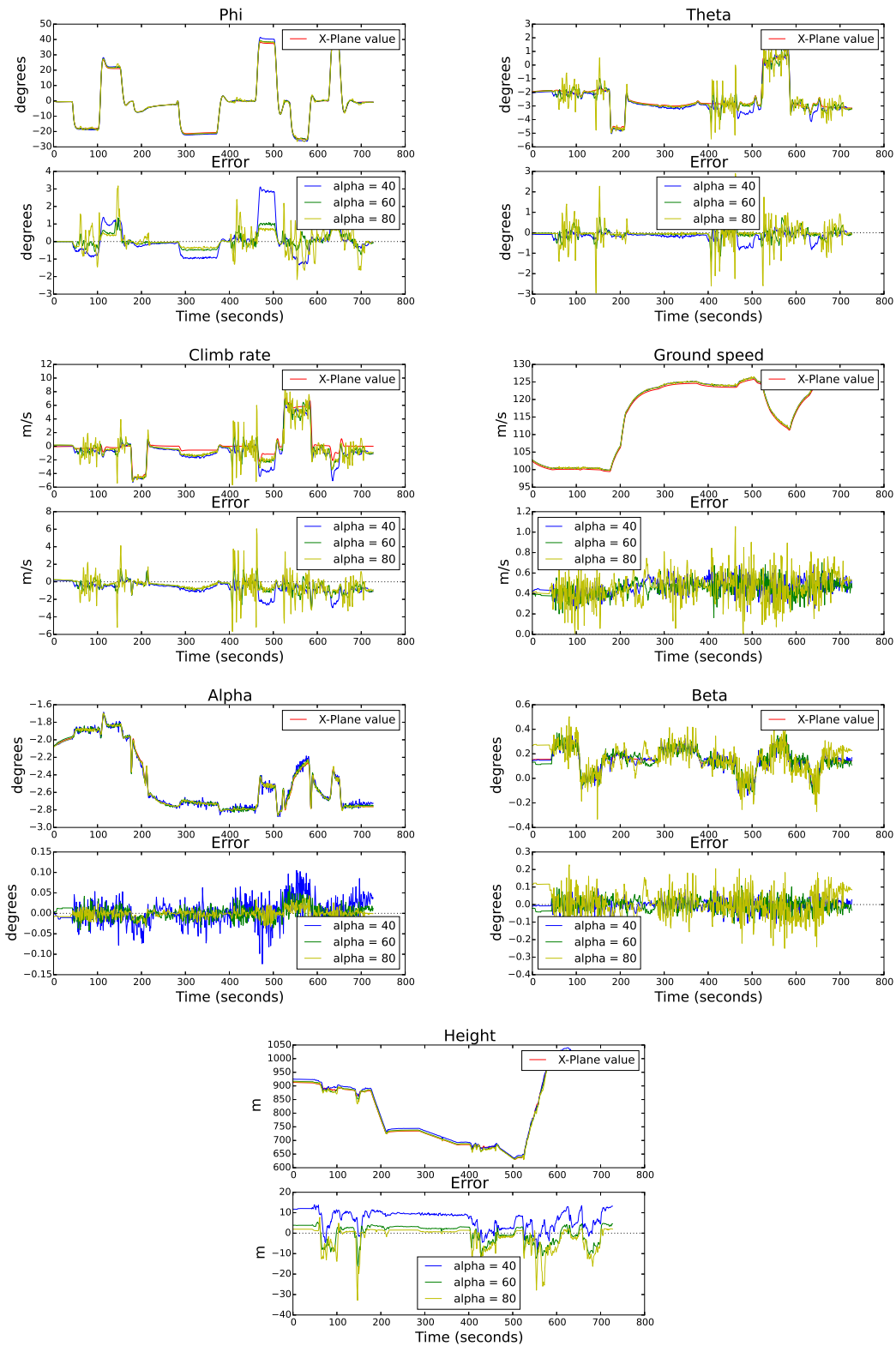


**Figure B-3:** The effect of  $\alpha_r$  on the states over a non-flat Earth. Three simulation are performed using Flight Data 1 where the configuration is J4 with  $\beta_r = 45^\circ$ . The value of  $\alpha_r$  is different for each simulation, and has values:  $40^\circ$ ,  $60^\circ$  and  $80^\circ$ .

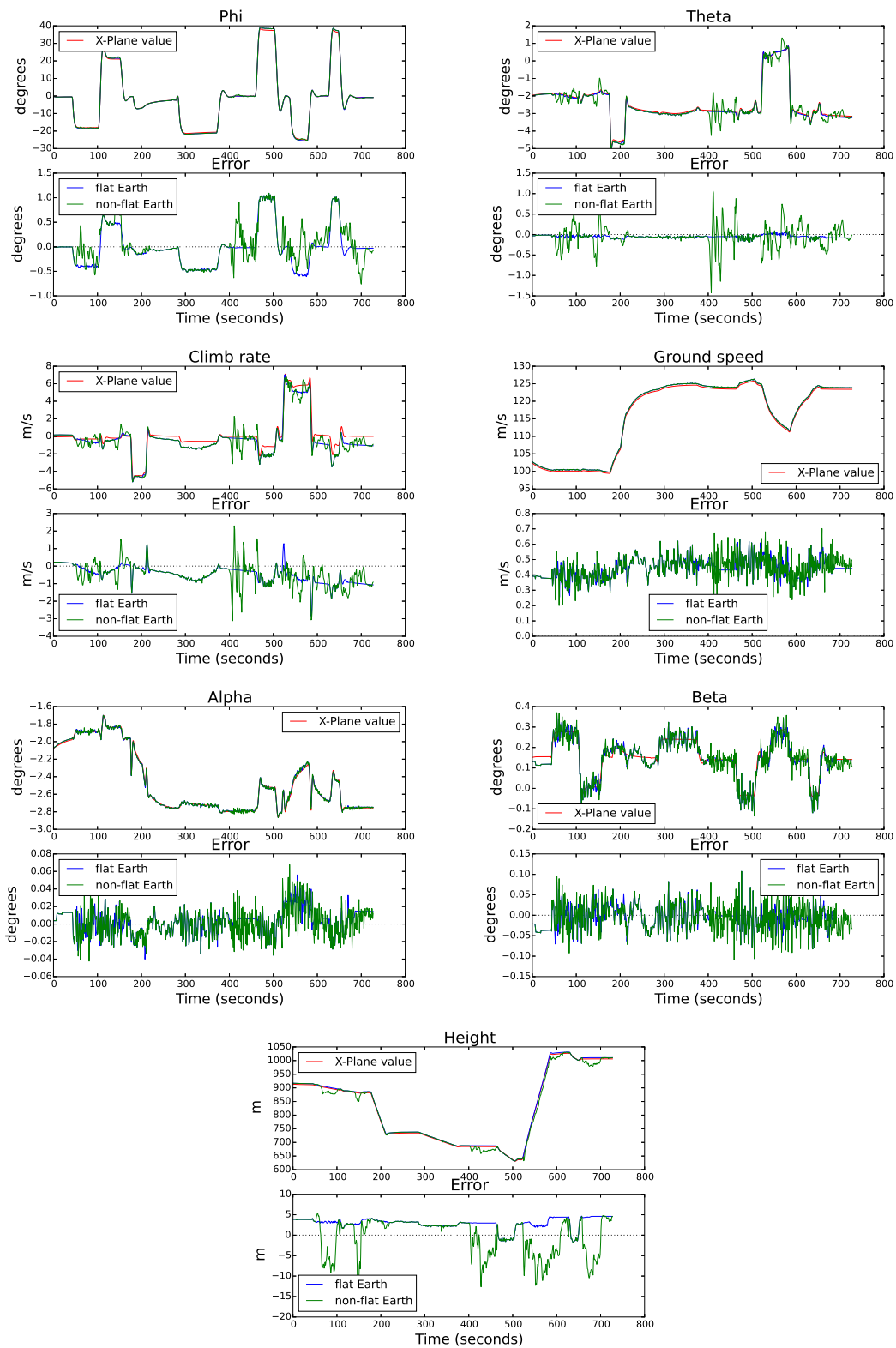


**Figure B-4:** The effect of terrain for the J4 configuration with  $\alpha_r = 60^\circ$  and  $\beta_r = 45^\circ$ . Two simulations are performed with FD 1, the only difference between the simulations is the DEM. In the first simulation the DEM is zero, and for the second it is the DEM of Holland.

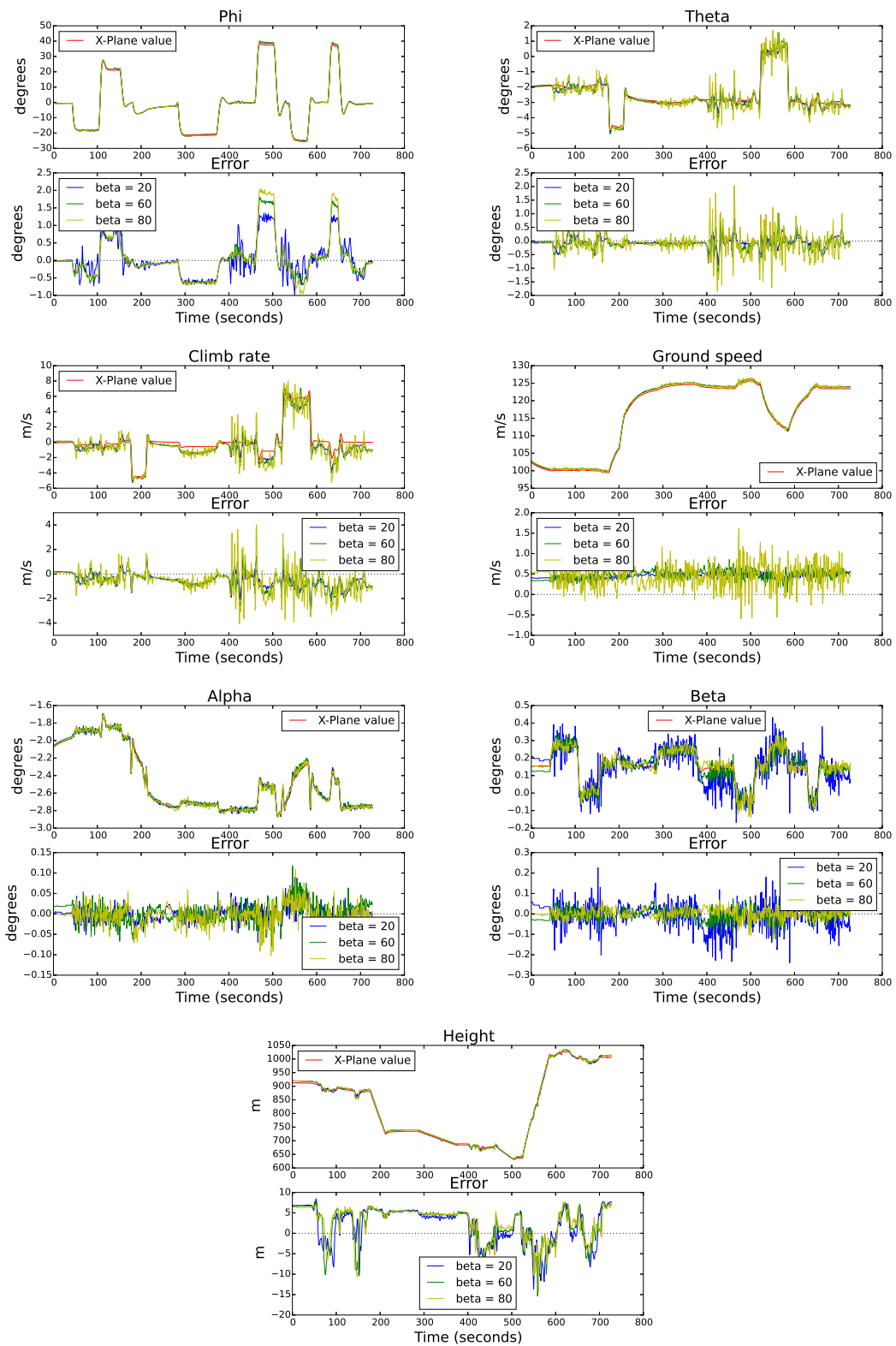


**Figure B-5:** The effect of  $\beta_r$  is measured with three simulations on non-flat terrain with FD 1. The configuration of each simulation is J4 with  $\alpha_r = 50^\circ$ .  $\beta_r$  is different for every simulation and has the values:  $20^\circ$ ,  $60^\circ$  and  $80^\circ$ .

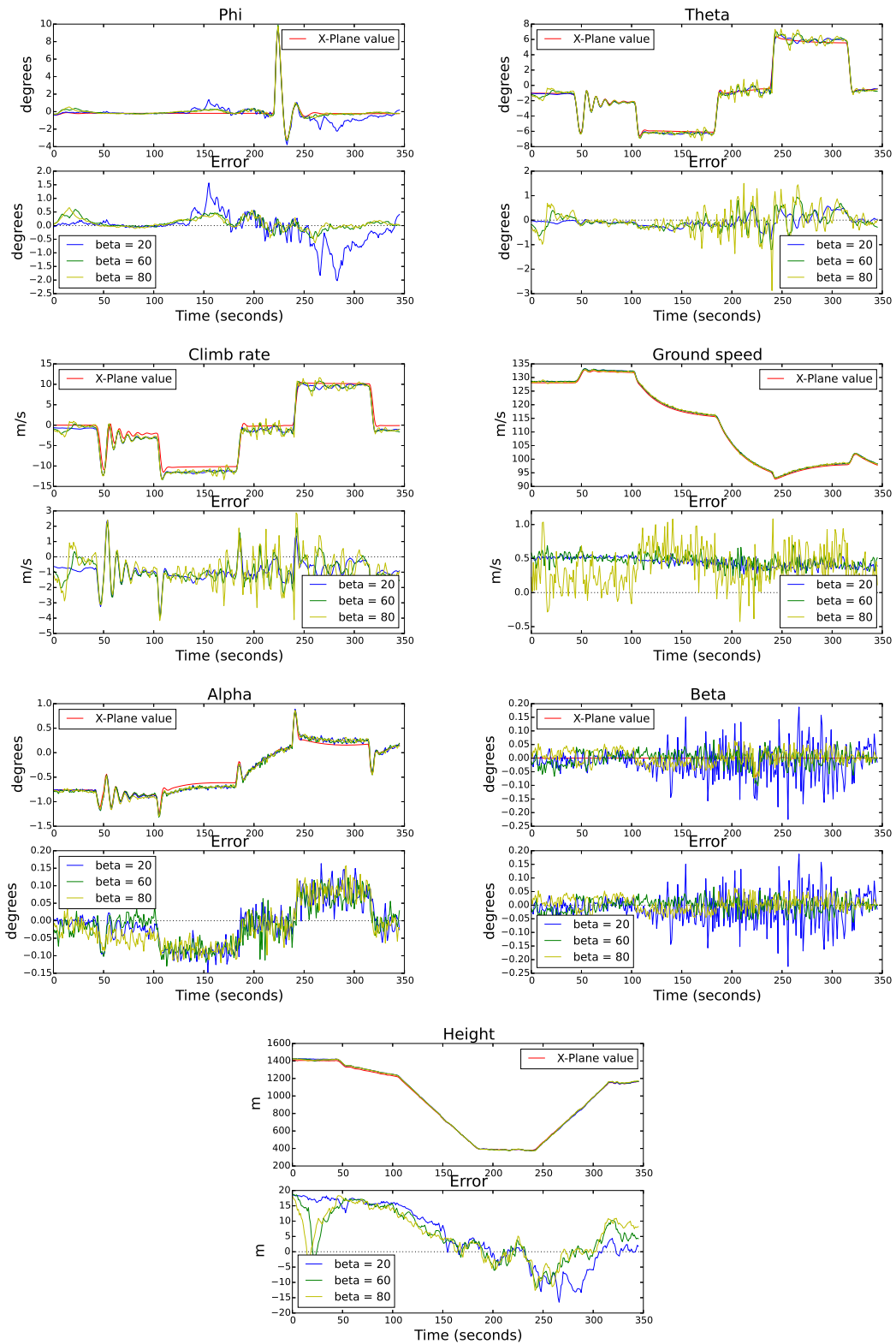


**Figure B-6:** The effect of  $\beta_r$  is measured with three simulations on non-flat terrain with FD 3. The configuration of each simulation is J4 with  $\alpha_r = 40^\circ$ .  $\beta_r$  is different for every simulation and has the values:  $20^\circ$ ,  $60^\circ$  and  $80^\circ$ .



---

## Appendix C

---

# Doppler ambiguity

The Nyquist theorem states that a signal should be sampled at a frequency at least twice as large as the frequency of the signal, giving the relation for the sample frequency  $f_s$ :

$$f_s = 2f_{signal} \quad (C-1)$$

The second Fourier transform is sampled with the PRF, the Nyquist theorem states therefore that the maximum unambiguous Doppler shift that can be measured is equal to:

$$f_{dmax} = \pm \frac{PRF}{2} \quad (C-2)$$

substituting the Doppler shift with Equation 3-5:

$$v_{max} = \frac{PRF}{4} \frac{c}{f_t} \quad (C-3)$$

A frequency that is not within the limits set by the Nyquist theorem will appear as a different frequency when the Fourier transform is performed. This is demonstrated in Figure C-1. The Fourier transform of a signal with frequency  $f_d$  is performed. However,  $f_d$  is less than  $-\frac{f_s}{2}$  and will therefore appear as  $f_a$  in the frequency spectrum, with  $f_a = f_d + f_s$ .

This means the PRF is an important factor which determines the maximum unambiguous velocity that can be measured by the radar. The maximum unambiguous velocity is  $38.22m/s$  for a radar with a  $PRF = 4892.4Hz$  and  $f_c = 9.6GHz$ . Figure C-2 shows two spectra, in Figure 3-5a the speed of the aircraft is  $50m/s$  and exceeds the maximum unambiguous velocity. Therefore the whole ground clutter is shifted by the PRF frequency. Figure C-2b shows the spectrum for an aircraft flying at  $25m/s$ .

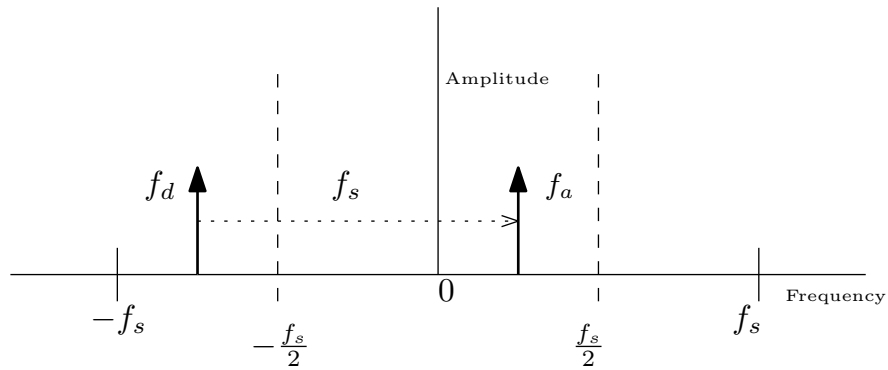


**Figure C-1:** This figure illustrates the principle of the Nyquist theorem with the corresponding shift.  $f_d$  is the measured Doppler shift however it is smaller than  $-PRF/2$ , therefore, it is measured as  $f_a$  instead.

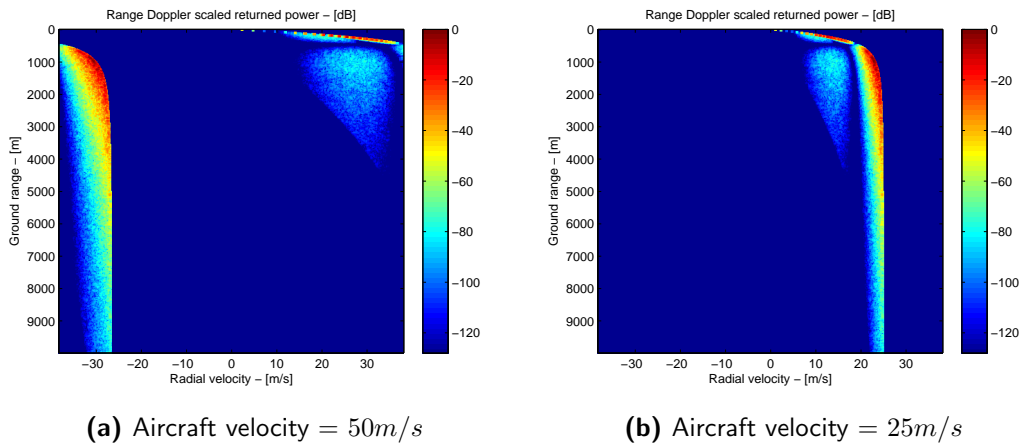


**Figure C-2:** Example of Doppler ambiguity in the VR spectrum. On the left, the relative radial velocity of the aircraft with respect to the ground exceeds the maximum unambiguous velocity the radar can measure. Therefore, a shift occurs in the spectrum. On the right, the aircraft velocity is within the limits so no shift occurs. As can be seen the limit in this case is  $38.22m/s$ .

---

## Bibliography

- Barrenechea, P., Elferink, F., & Janssen, J. (2007). Fmcw radar with broadband communication capability. In *Proceedings of 4th european radar conference* (p. 47).
- Dale, R. W., & Teresa, A. S. (2003, Fall). VFR Flight Into IMC: Reducing the Hazard. *Journal of Aviation/Aerospace Education and Research*, 13(1), 29-42.
- Diebel, J. (2006). Representing Attitude: Euler Angles, Unit Quaternions, and Rotation Vectors.
- FAA. (2014). FAA Pilot Handbook of Aeronautical Knowledge.
- Fried, W. R. (1956). Principles and Performance Analysis of Doppler Navigation Systems. *IRE Transactions on Aeronautical and Navigational Electronics*, December, 176–196.
- Fried, W. R. (1964). An FM-CW Radar for Simultaneous Three-Dimensional Velocity and Altitude Measurement. *IRE Transactions on Aeronautical and Navigational Electronics*, March, 45–57.
- Hyun, E., & Lee, J.-H. (2009). Method to improve range and velocity error using de-interleaving and frequency interpolation for automotive fmcw radars. *International Journal of Signal Processing, Image Processing and Pattern Recognition*, 2(2), 11–21.
- Hyun, E., Oh, W., & Lee, J.-H. (2012, May). Multi-target detection algorithm for fmcw radar. In *Radar conference (radar), 2012 ieee* (p. 0338-0341).
- ICAO. (1990). Annex 2 rules of the air.
- Pierrottet, D., Amzajerdian, F., Petway, L., Barnes, B., & Lockard, G. (2011). Flight test performance of a high precision navigation Doppler Lidar. *Sensors and Systems for Space Applications IV*, 8044.
- Pierrottet, D., Amzajerdian, F., Petway, L., Barnes, B., Lockard, G., & Rubio, M. (2008). Linear fmcw laser radar for precision range and vector velocity measurements. In *Symposium k materials and devices for laser remote sensing and optical communication* (Vol. 1076).
- Raney, R. (1971, May). Synthetic aperture imaging radar and moving targets. *Aerospace and Electronic Systems, IEEE Transactions on*, AES-7(3), 499-505.
- Skolnik, M. I. (2001). *Radar systems*. McGraw-Hill, NY.
- Undheim, R. (2012). *Design of a Linear FMCW Radar Synthesizer With Focus on Phase Noise*. Master of science thesis, Norwegian University of Science and Technology.

- Wojtkiewicz, A., Misiurewicz, J., Nałecz, M., Jedrzejewski, K., & Kulpa, K. (1997). Two-dimensional signal processing in FMCW radars. *Proc. XX KKTOiUE*, 475–480.